

Nonadiabatic Field with Triangle Window Functions on Quantum Phase Space

Xin He, Xiangsong Cheng, Baihua Wu, and Jian Liu*



Cite This: *J. Phys. Chem. Lett.* 2024, 15, 5452–5466



Read Online

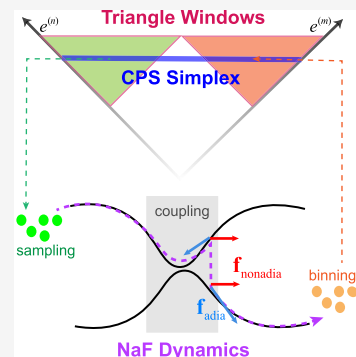
ACCESS |

Metrics & More

Article Recommendations

Supporting Information

ABSTRACT: Recent progress on the *constraint coordinate-momentum phase space* (CPS) formulation of finite-state quantum systems has revealed that the triangle window function approach is an isomorphic representation of the exact population–population correlation function of the two-state system. We use the triangle window (TW) function and the CPS mapping kernel element to formulate a novel useful representation of discrete electronic degrees of freedom (DOFs). When it is employed with nonadiabatic field (NaF) dynamics, a new variant of the NaF approach (i.e., NaF-TW) is proposed. The NaF-TW expression of the population of any adiabatic state is always positive semidefinite. Extensive benchmark tests of model systems in both the condensed phase and gas phase demonstrate that the NaF-TW approach is able to faithfully capture the dynamical interplay between electronic and nuclear DOFs in a broad region, including where the states remain coupled all the time, as well as where the bifurcation characteristic of nuclear motion is important.



Nonadiabatic transition dynamics is crucial in understanding many important light-driven, photoemission, charge transfer, and cavity modified phenomena in natural and artificial complex molecular systems in chemistry, materials, biology, quantum information and computation, environmental science, and so forth.^{1–14} In these systems, we often depict electrons by *discrete* electronic states and nuclei in continuous coordinate space. Numerical simulations of such composite systems often employ two prevailing categories of practical dynamics approaches with independent trajectories. The first category uses Born–Oppenheimer (BO) trajectories generated from different single-adiabatic-state potential energy surfaces (PESs). The surface hopping approach pioneered by Tully, Nikitin, and their co-workers^{15–19} has been modified by various hopping algorithms^{15–36} for connecting two independent Born–Oppenheimer trajectories on two different adiabatic PESs. The category of BO-trajectory-based dynamics often meets the challenge for nonadiabatic processes where the states remain coupled all the time, especially when the temperature is relatively low. Another category utilizes the independent mean field trajectory in the spirit of the Ehrenfest theorem.³⁷ In addition to the original Ehrenfest dynamics³⁷ for nonadiabatic transitions,^{38–40} a few Ehrenfest-like dynamics approaches^{41–62} pioneered by Miller and co-workers^{41,42} have been developed, especially since the Meyer–Miller mapping Hamiltonian model was proposed for treating both nuclear and electronic degrees of freedom (DOFs) on the same footing.^{42,63} Among these Ehrenfest-like dynamics approaches, the symmetrical quasi-classical (SQC) method for nonadiabatic dynamics^{53–55,57,58} is of particular interest. In the latest version of the SQC method, Cotton and Miller introduced the triangle window function (TWF) approach for discrete electronic

DOFs.^{54,57,58} The TWF approach, albeit proposed as a heuristic empirical model, is reasonably accurate for electronic dynamics (in the frozen-nuclei limit) even in the weak state–state coupling region.⁵⁴ In addition to the TWF approach offering the initial condition as well as the integral expression of the time-dependent physical property for electronic DOFs, the independent quasi-classical trajectory is generated from Ehrenfest-like dynamics of the Meyer–Miller mapping Hamiltonian.⁴² The SQC with TWF for nonadiabatic dynamics^{54,55,57} has widely been applied to various condensed phase system-bath models as well as realistic molecular systems.^{58,64–72} The category of independent mean field trajectory-based dynamics methods performs well in the nonadiabatic state–state coupling region but is more difficult in capturing the bifurcation characteristic of the nuclear motion in the asymptotic region where the state–state coupling disappears. It is shown in refs 50 and 73 that the interference between different mean field trajectories (e.g., in the forward–backward or fully semiclassical initial value representation framework^{74–76}) is necessary for describing the correct nuclear dynamics behavior in the asymptotic region, which requests more computational effort. In addition to the two major categories, there are some other methods using independent trajectories.^{77–81}

Received: March 14, 2024

Revised: April 29, 2024

Accepted: May 1, 2024

The unified phase space formulation with coordinate-momentum variables offers an exact interpretation of quantum mechanics to describe composite systems,^{82–90} where the *constraint* coordinate-momentum *phase space* (CPS) representation is used for *discrete* (electronic) degrees of freedom (DOFs) while the infinite (Wigner) coordinate-momentum phase space representation is used for *continuous* (nuclear) DOFs. The CPS representation (of discrete electronic DOFs) related to the quotient space $U(F)/U(F - 1)$ was first introduced to nonadiabatic dynamics for general F -state systems by the sphere representation with coordinate-momentum variables in Section II of ref 84 and by the simplex representation with action-angle variables in Appendix A of ref 84. It was shortly developed to a generalized phase space formulation, CPS with commutator variables^{86,87} in spirit of refs 82–84, which is related to the quotient space $U(F)/U(F - r)$ (with $1 \leq r < F$), namely, the complex Stiefel manifold.^{91–93} As discussed in Appendix 3 of ref 88, the exact equations of motion (EOMs) of mapping coordinate-momentum variables of CPS for the pure finite-state quantum system are linear,^{82–85} which is superior to the conventional phase space approaches with angle variables^{94–97} used in physics for studying dynamics of composite systems.^{98–102} More importantly, the CPS formulation offers a powerful framework to derive more new (isomorphic) representations of the finite-state quantum system. This is demonstrated in ref 103 and in the present Letter.

The unified phase space formulation has recently led to a conceptually novel trajectory-based approach in the adiabatic representation of electronic states, nonadiabatic field (NaF) that is promising in faithfully describing both nuclear motion and electronic coherence/dissipation.¹⁰⁴ In the state–state coupling region, the nuclear EOMs of the independent trajectory of NaF involve an important nonadiabatic nuclear force term in addition to an adiabatic nuclear force term of a single electronic state (either stochastically with electronic weights or deterministically with the dominant electronic weight). This is substantially different from the two conventional categories of nonadiabatic dynamics methods that involve either BO trajectories on different PESs or mean field trajectories.

The NaF strategy¹⁰⁴ has been applied to the framework of Ehrenfest dynamics,³⁷ fewest-switches surface hopping (FSSH),^{15,16} and CPS with commutator variables.^{84,86–88,105} The investigation suggests that the nuclear EOMs of the NaF strategy should considerably improve over various surface hopping and Ehrenfest-like dynamics methods. It also indicates that the key of the most successful NaF approach includes the exact phase space representation of discrete electronic DOFs,¹⁰⁴ which offers a consistent way in dealing with the other two critical properties of a trajectory-based quantum dynamics method,⁸⁸ namely, the initial condition of the trajectory and the integral expression for evaluation of the time-dependent physical property.

In this Letter, we employ triangle window functions,⁵⁴ in addition to the original mapping kernel of the $U(F)/U(F - 1)$ CPS,^{84,85} to formulate a novel representation of discrete (electronic) DOFs, which is applied with the NaF strategy to offer a more consistent trajectory-based approach for studying nonadiabatic transition dynamics.

Assume a coupled F -electronic-state Hamiltonian operator of the composite system

$$\hat{H} = \sum_{n,m=1}^F H_{nm}(\mathbf{R}, \mathbf{P}) |n\rangle\langle m| \quad (1)$$

where $\{\mathbf{R}, \mathbf{P}\}$ are the coordinate and momentum variables for the nuclear DOFs, and $\{|n\rangle\}$, $n \in \{1, \dots, F\}$ is the “complete” set of orthonormal electronic states (F is in general infinite when the set of electronic states is rigorously complete). Consider the composite system in the frozen-nuclei limit of eq 1, where each element $H_{nm}(\mathbf{R}, \mathbf{P}) \equiv H_{nm}$ is constant and the Hamiltonian operator of eq 1 becomes $\hat{H} = \sum_{n,m=1}^F H_{nm} |n\rangle\langle m|$, which is the pure F -state quantum system. A generalization of the idea of the exact weighted CPS representation of ref 88 implies that the integrand function on electronic mapping CPS is not limited to the product of the element of the mapping kernel and that of the inverse mapping kernel of electronic DOFs.¹⁰³ The general phase space expression of the time correlation function between $|n\rangle\langle m|$ and $|k\rangle\langle l|$ reads

$$\text{Tr}_e[|n\rangle\langle m| e^{i\hat{H}t} |k\rangle\langle l| e^{-i\hat{H}t}] = (C_{nm,kl}(t))^{-1} \int d\gamma w(\gamma) \times \int_{S(\mathbf{x}, \mathbf{p}, \Gamma; \gamma)} F dx dp d\Gamma Q_{nm,kl}(\mathbf{x}, \mathbf{p}, \Gamma; \gamma; t) \quad (2)$$

where $\text{Tr}_e[\cdot]$ represents the trace over electronic DOFs, $\{\mathbf{x}, \mathbf{p}\} = \{\mathbf{x}^{(1)}, \dots, \mathbf{x}^{(F)}, \mathbf{p}^{(1)}, \dots, \mathbf{p}^{(F)}\}$ are the mapping coordinate and momentum variables for discrete electronic DOFs, and Γ is the $F \times F$ commutator matrix^{82,86} that can be expressed by auxiliary coordinate-momentum variables,

$$\Gamma_{mn} = \sum_{k=1}^F s_k (\xi_k^{(m)} + i\pi_k^{(m)}) (\xi_k^{(n)} - i\pi_k^{(n)}) / 2 \quad (3)$$

In eq 2, $F dx dp d\Gamma$ with $d\Gamma = \prod_{k,m=1}^F d\xi_k^{(m)} d\pi_k^{(m)}$ is the integral measure, $S(\mathbf{x}, \mathbf{p}, \Gamma; \gamma)$ defines the phase space constraint that involves parameters γ , $w(\gamma)$ is the quasi-distribution of parameter vector γ , and $C_{nm,kl}(t)$ is the time-dependent normalization factor. $Q_{nm,kl}(\mathbf{x}, \mathbf{p}, \Gamma; \gamma; t)$ defines the integrand function on the phase space corresponding to $|n\rangle\langle m|$ at time 0 and $e^{i\hat{H}t}|k\rangle\langle l|e^{-i\hat{H}t}$ at time t , which is a generalization of $K_{mn}(\mathbf{x}, \mathbf{p}, \Gamma) K_{kl}^{-1}(\mathbf{x}, \mathbf{p}, \Gamma; t)$, the product of the element of the mapping kernel and that of its inverse mapping kernel of our CPS formulations.^{82–89,93,106} (The convention $\hbar = 1$ is used for discrete electronic DOFs throughout this Letter and its Supporting Information.)

The general expression of the time correlation function eq 2 with trajectory-based dynamics becomes

$$\text{Tr}_e[|n\rangle\langle m| e^{i\hat{H}t} |k\rangle\langle l| e^{-i\hat{H}t}] \mapsto (\bar{C}_{nm,kl}(t))^{-1} \int w(\gamma) dy \times \int_{S(\mathbf{x}_0, \mathbf{p}_0, \Gamma_0; \gamma)} F dx_0 dp_0 d\Gamma_0 \bar{Q}_{nm,kl}(\{\mathbf{x}, \mathbf{p}, \Gamma\}_{0 \leq \tau \leq t}; \gamma; t) \quad (4)$$

where $\{\mathbf{x}, \mathbf{p}, \Gamma\}_{0 \leq \tau \leq t}$ denotes the trajectory on the phase space, $\bar{Q}_{nm,kl}(\{\mathbf{x}, \mathbf{p}, \Gamma\}_{0 \leq \tau \leq t}; \gamma; t)$ defines the integrand function on the phase space corresponding to $|n\rangle\langle m|$ at time 0 and $e^{i\hat{H}t}|k\rangle\langle l|e^{-i\hat{H}t}$ at time t for trajectory dynamics, and $\bar{C}_{nm,kl}(t)$ is the time-dependent normalization factor of the trajectory-based dynamics approach. The expression of eq 4 is a generalization of the formalisms in the CPS formulation,^{82–89,93,106} where the trajectory is generated by the linear EOMs yielded from the symplectic structure of CPS.

Our recent work of ref 103 presents a new class of isomorphic representations of the exact population–population correlation function of the pure two-state quantum system (i.e., $F = 2$). Remarkably, the TWF approach (for discrete electronic DOFs) originally proposed as a heuristic empirical model by Cotton and Miller,⁵⁴ is proved as a special case of the new class of phase space representations for *exact* population dynamics.¹⁰³ The proof involves the projection of the TWF onto the $U(F)/U(F - 1)$ CPS for the two-state system and integral identities for the exact population–population correlation function. Because the TWF approach is exact for the population dynamics of the two-state system¹⁰³ and reasonably accurate for that of the multistate system (i.e., $F \geq 3$),⁵⁴ it suggests that the triangle window function should be valuable for developing a novel useful representation of discrete electronic DOFs (e.g., for nonadiabatic dynamics).

Consider the pure F -state system of eq 1. We focus on a special class of eq 4,

$$\begin{aligned} \text{Tr}_e[|n\rangle\langle m|e^{i\hat{H}t}|k\rangle\langle l|e^{-i\hat{H}t}] &\mapsto (\bar{C}_{nm,kl}(t))^{-1} \int d\gamma w(\gamma) \\ &\times \int_{S(x_0, p_0; \Gamma_0; \gamma)} F dx_0 dp_0 d\Gamma_0 \bar{Q}_{nm,kl}(x_0, p_0, \Gamma_0; x_t, p_t, \Gamma_t) \end{aligned} \quad (5)$$

Equation 5 includes four kinds of time correlation functions of electronic DOFs, namely, population–population ($n = m$ and $k = l$), population–coherence ($n = m$ and $k \neq l$), coherence–population ($n \neq m$ and $k = l$), and coherence–coherence ($n \neq m$ and $k \neq l$) correlation functions. Commutator matrix Γ can be constant, that is, $\Gamma = \gamma \mathbf{1}$, where γ is a scalar parameter and $\mathbf{1}$ is the identity matrix. In this case, the constraint of CPS reads

$$S(x, p; \gamma) = \delta \left(\sum_{n=1}^F \frac{1}{2} ((x^{(n)})^2 + (p^{(n)})^2) - (1 + F\gamma) \right) \quad (6)$$

with parameter $\gamma \in (-1/F, \infty)$, and

$$\begin{aligned} &\int_{S(x, p; \gamma)} F dx dp g(x, p) \\ &= \int F dx dp \frac{1}{\Omega(\gamma)} S(x, p; \gamma) g(x, p) \end{aligned} \quad (7)$$

where $\Omega(\gamma)$ is the normalization factor^{84,85,88}

$$\Omega(\gamma) = \int dx dp S(x, p; \gamma) = \frac{(2\pi)^F (1 + F\gamma)^{F-1}}{(F-1)!} \quad (8)$$

By employing a generalization of the weighted constraint phase space,⁸⁸ the expressions of time correlation functions read

$$\begin{aligned} \text{Tr}_e[|n\rangle\langle m|e^{i\hat{H}t}|k\rangle\langle l|e^{-i\hat{H}t}] &\mapsto (\bar{C}_{nm,kl}(t))^{-1} \int_{-1/F}^{+\infty} w(\gamma) d\gamma \\ &\times \int_{S(x_0, p_0; \gamma)} F dx_0 dp_0 \bar{Q}_{nm,kl}(x_0, p_0; x_t, p_t) \end{aligned} \quad (9)$$

For example, the CMM approach of ref 69 can be reinterpreted by eq 9 with $w(\gamma) = \delta(\gamma - \gamma_0)$ and $\bar{Q}_{nm,kl}(x_0, p_0; x_t, p_t) = K_{mn}(x_0, p_0) K_{lk}^{-1}(x_t, p_t)$, where $K_{mn}(x, p)$ and $K_{lk}^{-1}(x, p)$ are matrix elements of eqs 7 and 8 of ref 69 with phase space parameter γ_0 , respectively. In this Letter, we employ the TWF⁵⁴ for the integral expression of the electronic correlation function. The unified expression reads

$$\begin{aligned} \text{Tr}_e[|n\rangle\langle m|e^{i\hat{H}t}|k\rangle\langle l|e^{-i\hat{H}t}] &\mapsto (\bar{C}_{nm,kl}(t))^{-1} \int_0^{1-1/F} w(\gamma) d\gamma \\ &\times \int_{S(x_0, p_0; \gamma)} F dx_0 dp_0 \bar{Q}_{nm,kl}(x_0, p_0; x_t, p_t) \\ &= (\bar{C}_{nm,kl}(t))^{-1} \int dx_0 dp_0 \frac{F \cdot F!}{(2\pi)^F (F^F - 1)} \bar{Q}_{nm,kl}(x_0, p_0; x_t, p_t) \end{aligned} \quad (10)$$

where $w(\gamma) = \frac{F^2}{F^F - 1} (1 + F\gamma)^{F-1}$ and $\int_0^{1-1/F} w(\gamma) d\gamma = 1$. In the expression of $\text{Tr}_e[|n\rangle\langle m|e^{i\hat{H}t}|l\rangle\langle l|e^{-i\hat{H}t}]$ of eq 10,

$$\begin{aligned} &\bar{Q}_{nn,mm}(x_0, p_0; x_t, p_t) \\ &= \bar{w}_n^{\text{SOC}}(x_0, p_0) K_{mm}^{\text{SOC}}(x_0, p_0) K_{mm}^{\text{bin}}(x_t, p_t) \end{aligned} \quad (11)$$

where

$$\bar{w}_n^{\text{SOC}}(x_0, p_0) = \frac{2(F^F - 1)}{F \cdot F!} \left(2 - \frac{1}{2} ((x_0^{(n)})^2 + (p_0^{(n)})^2) \right)^{2-F} \quad (12)$$

The time-dependent normalization factor reads

$$\begin{aligned} \bar{C}_{nn,mm}(t) &= \sum_{k=1}^F \int_0^{1-1/F} w(\gamma) d\gamma \\ &\times \int_{S(x_0, p_0; \gamma)} F dx_0 dp_0 \bar{Q}_{nn,kk}(x_0, p_0; x_t, p_t) \\ &= \sum_{k=1}^F \int dx_0 dp_0 \frac{F \cdot F!}{(2\pi)^F (F^F - 1)} \bar{Q}_{nn,kk}(x_0, p_0; x_t, p_t) \end{aligned} \quad (13)$$

whose initial value $\bar{C}_{nn,mm}(0)$ is 1. For $n \neq m$ or $k \neq l$, $\bar{C}_{nn,kl}(t) \equiv 1$. The TWF for $|n\rangle\langle n|$, the population of the n -th state at time 0, is an indicator function,

$$K_{nn}^{\text{SOC}}(x_0, p_0) \equiv \begin{cases} 1 & \text{if } (x_0, p_0) \in \mathcal{M}_n \\ 0 & \text{otherwise} \end{cases} \quad (14)$$

where \mathcal{M}_n includes the following set of phase space points,

$$\mathcal{M}_n(x, p) : \left\{ (x, p) \middle| \begin{array}{l} 1 \leq \frac{1}{2} ((x^{(n)})^2 + (p^{(n)})^2) \leq 2 \\ \forall k \neq n, \frac{1}{2} ((x^{(k)})^2 + (p^{(k)})^2) + (x^{(n)})^2 + (p^{(n)})^2 \leq 2 \end{array} \right\} \quad (15)$$

For any point (x, p) in $\mathcal{M}_n(x, p)$, the value of $\sum_{n=1}^F \frac{1}{2} ((x^{(n)})^2 + (p^{(n)})^2)$ lies in region $[1, F]$, so that the domain of γ is $\gamma \in [0, 1 - 1/F]$. The TWF for $e^{i\hat{H}t}|m\rangle\langle m|e^{-i\hat{H}t}$, the population of the m -th state at time t , is also an indicator function,

$$K_{mm}^{\text{bin}}(x_t, p_t) \equiv \begin{cases} 1 & \text{if } (x_t, p_t) \in \mathcal{M}_m^{\text{bin}} \\ 0 & \text{otherwise} \end{cases} \quad (16)$$

where

$$\mathcal{M}_m^{\text{bin}}(x, p) : \left\{ (x, p) \middle| \begin{array}{l} 1 \leq \frac{1}{2} ((x^{(m)})^2 + (p^{(m)})^2) \\ \forall k \neq m, \frac{1}{2} ((x^{(k)})^2 + (p^{(k)})^2) \leq 1 \end{array} \right\} \quad (17)$$

Because functions $K_{nn}^{\text{SOC}}(x_0, p_0)$ and $K_{mm}^{\text{bin}}(x_t, p_t)$ of eq 10 and eq 13 are always non-negative, the population–population

correlation function remains positive semidefinite all the time for the choice of the electronic basis set $\{|n\rangle\}$ of eq 1. The expression of eq 10 for the population–population correlation function is exact for only the pure two-state system. We note that the phase space formalism of eqs 10 and 11 is not the only option, and an alternative formulation derived for triangle window functions is presented in Section S5 of the Supporting Information.

Unfortunately, the SQC approach with either triangle or square window functions^{54,107} does not lead to exact results for the other three kinds of electronic correlation functions even for the pure two-state case ($F = 2$). It is crucial to construct the new phase space representation with the triangle window function used in eqs 14 and 15 for the initial condition such that the other three kinds of electronic correlation functions are exact. Here, we employ the element of the mapping kernel of the U(F)/U($F - 1$) CPS^{84,85} to accomplish the task.

In the expression of eq 10 for $\text{Tr}_e[|n\rangle\langle n|e^{i\hat{H}t}|k\rangle\langle l|e^{-i\hat{H}t}]$ with $k \neq l$, the population–coherence correlation function,

$$\bar{Q}_{nm,kl}(\mathbf{x}_0, \mathbf{p}_0; \mathbf{x}_t, \mathbf{p}_t) = \bar{w}_n^{\text{SOC}}(\mathbf{x}_0, \mathbf{p}_0) K_{nn}^{\text{SOC}}(\mathbf{x}_0, \mathbf{p}_0) K_{lk}^{\text{CMM}}(\mathbf{x}_t, \mathbf{p}_t) \quad (18)$$

where

$$K_{lk}^{\text{CMM}}(\mathbf{x}_t, \mathbf{p}_t) \equiv \frac{1}{2}(x_t^{(l)} + ip_t^{(l)})(x_t^{(k)} - ip_t^{(k)}) \quad (19)$$

is the element of the mapping kernel of the U(F)/U($F - 1$) CPS.^{84,85} The time-dependent normalization factor of eq 5 is constant, $\bar{C}_{nn,kl}(t) \equiv 1$. When the initial electronic density matrix includes the coherence term, $|n\rangle\langle m|$ (where $n \neq m$), in the expression of eq 10 for both the coherence–population (where $n \neq m$ and $k = l$) and coherence–coherence (where $n \neq m$ and $k \neq l$) correlation functions,

$$\bar{Q}_{nm,kl}(\mathbf{x}_0, \mathbf{p}_0; \mathbf{x}_t, \mathbf{p}_t) = \bar{w}_{nm}^{\text{coh}}(\mathbf{x}_0, \mathbf{p}_0) K_{nn}^{\text{CMM}}(\mathbf{x}_0, \mathbf{p}_0) K_{lk}^{\text{CMM}}(\mathbf{x}_t, \mathbf{p}_t) \quad (20)$$

where $\bar{w}_{nm}^{\text{coh}}(\mathbf{x}_0, \mathbf{p}_0) = \sum_{i=n,m}^6 \bar{w}_i^{\text{SOC}}(\mathbf{x}_0, \mathbf{p}_0) K_{ii}^{\text{SOC}}(\mathbf{x}_0, \mathbf{p}_0)$ involves the triangle window functions for the n -th and m -th states at time 0. The time-dependent normalization factor $\bar{C}_{nm,kl}(t) \equiv 1$ for $n \neq m$ is also a constant.

The new electronic representation of eq 10 for evaluation of the electronic density matrix at time t , which is denoted as the CPS with triangle window functions (CPS-TW) approach. It has three important properties:

- 1) In the frozen-nuclei limit, the representation of the electronic population–population correlation is exact for the two-state system ($F = 2$) and is expected to be reasonably accurate for the multistate system ($F \geq 3$). (See more discussion in ref 103.)
- 2) The representation of the other three kinds of correlation functions yields the exact frozen-nuclei limit for all cases ($F \geq 2$). (See more discussion in Section S1 of the Supporting Information.)
- 3) When the phase space expression of the total density operator of both electronic and nuclear DOFs is initially non-negative, the expression of the electronic population–population correlation (eq 10) is guaranteed to be positive semidefinite for all cases ($F \geq 2$).

In comparison to the exact CPS representations of electronic DOFs, the third property (of the CPS-TW approach) is indispensable for solving the negative population problem of phase space mapping dynamics methods for general F -state systems, e.g., as shown in Figures 4 and 7 of ref 86 and in Figure S12 of the Supporting Information of ref 104. In addition to the TWF approach, other cases of the novel class of phase space representations introduced in ref 103 can also be utilized with the CPS formulation to offer the integral expression for the four kinds of electronic correlation functions, which is expected to have the same properties of the CPS-TW approach.

By employing the CPS-TW approach instead of the exact CPS representations for electronic DOFs, in addition to using the infinite Wigner coordinate-momentum phase space for nuclear DOFs, we obtain the expression of the correlation function for both electronic and nuclear DOFs

$$\begin{aligned} & \text{Tr}_{n,c}[(|n\rangle\langle m| \otimes \hat{\rho}_{\text{nuc}}) e^{i\hat{H}t/\hbar} (|k\rangle\langle l| \otimes \hat{A}_{\text{nuc}}) e^{-i\hat{H}t/\hbar}] \\ & \mapsto (\bar{C}_{nm,kl}(t))^{-1} (2\pi\hbar)^{-N} \int d\mathbf{R}_0 d\mathbf{p}_0 \int_0^{1-1/F} w(\gamma) d\gamma \\ & \times \int_{S(\mathbf{x}_0, \mathbf{p}_0; \gamma)} F d\mathbf{x}_0 d\mathbf{p}_0 \rho_W(\mathbf{R}_0, \mathbf{p}_0) A_W(\mathbf{R}_t, \mathbf{p}_t) \bar{Q}_{nm,kl}(\mathbf{x}_0, \mathbf{p}_0; \mathbf{x}_t, \mathbf{p}_t) \end{aligned} \quad (21)$$

Here, $\text{Tr}_{n,c}[\cdot]$ represents the trace over nuclear DOFs, $\rho_W(\mathbf{R}, \mathbf{P})$ and $A_W(\mathbf{R}, \mathbf{P})$ are the Wigner phase space functions of nuclear operators $\hat{\rho}_{\text{nuc}}$ and \hat{A}_{nuc} , respectively. For instance, $A_W(\mathbf{R}, \mathbf{P}) = \int d\Delta \langle \mathbf{R} - \Delta/2 | \hat{A}_{\text{nuc}} | \mathbf{R} + \Delta/2 \rangle \exp(-i\Delta \cdot \mathbf{P}/\hbar)$. In addition, when nuclear DOFs are also considered,

$$\begin{aligned} \bar{C}_{nn,mm}(t) = & \sum_{k=1}^F (2\pi\hbar)^{-N} \int d\mathbf{R}_0 d\mathbf{p}_0 \int_0^{1-1/F} w(\gamma) d\gamma \\ & \times \int_{S(\mathbf{x}_0, \mathbf{p}_0; \gamma)} F d\mathbf{x}_0 d\mathbf{p}_0 \rho_W(\mathbf{R}_0, \mathbf{p}_0) \bar{Q}_{nn,kk}(\mathbf{x}_0, \mathbf{p}_0; \mathbf{x}_t, \mathbf{p}_t) \end{aligned} \quad (22)$$

Provided that eq 21 is the integral expression of the time-dependent property, we propose a new variant of the NaF approach, namely, NaF with triangle window functions (NaF-TW), in the adiabatic representation (of electronic states).

Consider the full Hamiltonian of nuclei and electrons of the system

$$\begin{aligned} \hat{H} = & \frac{1}{2} \hat{\mathbf{P}}^T \mathbf{M}^{-1} \hat{\mathbf{P}} + \hat{H}_{\text{el}}(\hat{\mathbf{R}}) \\ = & \frac{1}{2} \hat{\mathbf{P}}^T \mathbf{M}^{-1} \hat{\mathbf{P}} + \sum_k E_k(\mathbf{R}) |\phi_k(\mathbf{R})\rangle\langle\phi_k(\mathbf{R})| \end{aligned} \quad (23)$$

where $\mathbf{M} = \text{diag}\{m_i\}$ is the diagonal nuclear mass matrix, $\hat{H}_{\text{el}}(\hat{\mathbf{R}})$ is the electronic Hamiltonian that includes the kinetic energy of electrons and all the electrostatic potential among electrons and nuclei, and $E_k(\mathbf{R})$ denotes the adiabatic PES of the k -th adiabatic electronic state, $|\phi_k(\mathbf{R})\rangle$. The expression of the right-hand side (RHS) for the full Hamiltonian operator of eq 23 was first employed for phase space mapping methods for nonadiabatic dynamics in refs 88 and 108. The nonadiabatic coupling vector in the adiabatic representation is $\mathbf{d}_{mn}(\mathbf{R}) = \left\langle \phi_m(\mathbf{R}) \left| \frac{\partial \phi_n(\mathbf{R})}{\partial \mathbf{R}} \right. \right\rangle$, of which the J -th component is $d_{mn}^{(J)}(\mathbf{R})$. Note that $-i\mathbf{d}^{(J)}(\mathbf{R})$ is a Hermitian matrix of electronic DOFs and that vector $-i\mathbf{d}(\mathbf{R})$ implies a nonabelian gauge field.^{88,109} Assume that $\{|\phi_n\rangle\}$, $n \in \{1, \dots, F\}$, are effectively complete to describe the process where the gauge field tensor,

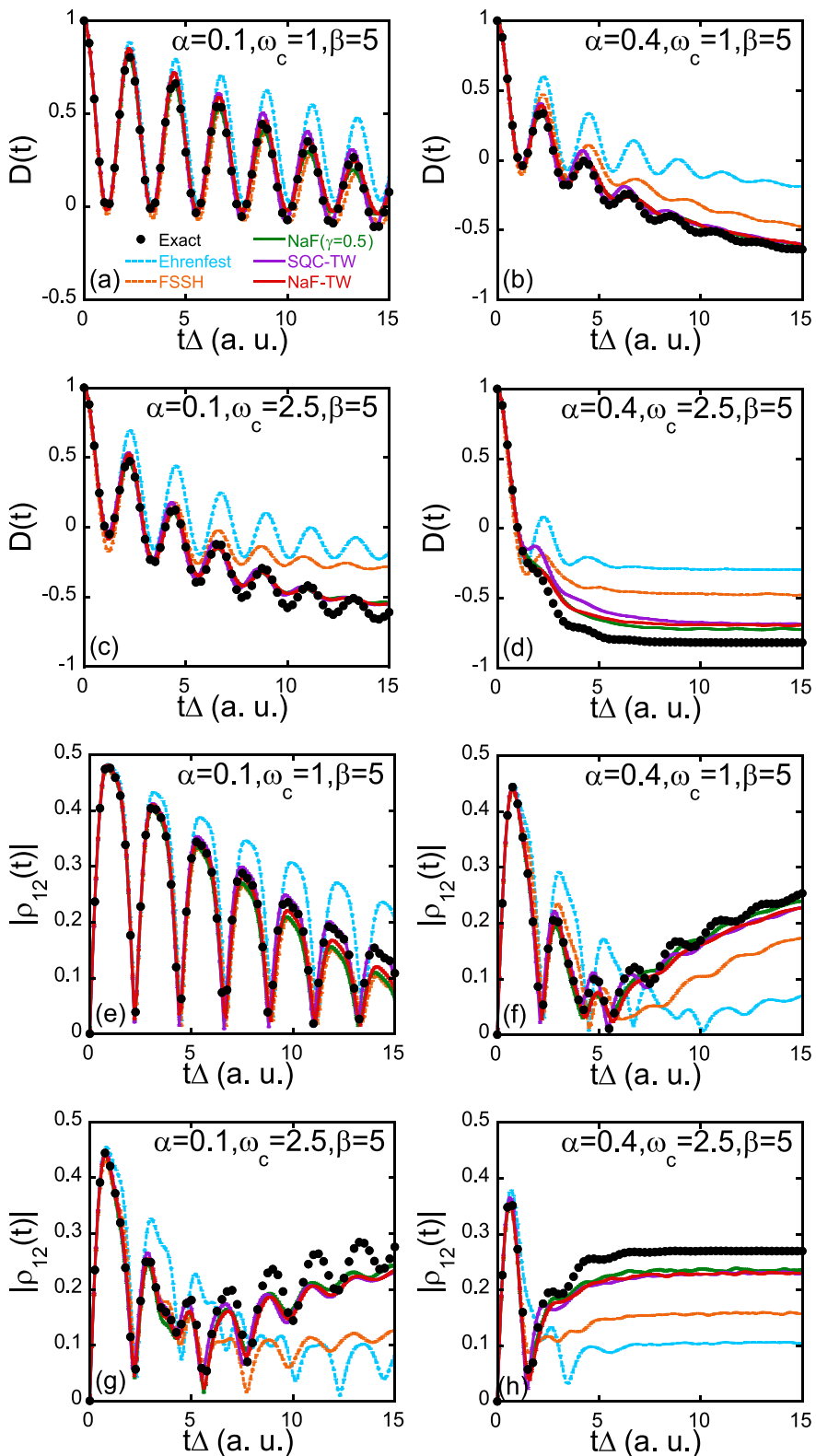


Figure 1. Panels (a–d): The population difference between State 1 and State 2, $D(t)$, as a function of time for the four spin-boson models with the Ohmic spectral density at the inverse temperature $\beta = 5$. Panels (e–h): The modulus of the off-diagonal (coherence) element of the reduced electronic density matrix, $|\rho_{12}(t)|$, as a function of time. Panels (a–d) or (e–h) represent the results of the spin-boson models with parameters $\{\alpha = 0.1, \omega_c = 1\}$, $\{\alpha = 0.4, \omega_c = 1\}$, $\{\alpha = 0.1, \omega_c = 2.5\}$, and $\{\alpha = 0.4, \omega_c = 2.5\}$, respectively. Black points: (exact results produced by) eHEOM. Cyan long-dashed lines: Ehrenfest dynamics. Orange short-dashed lines: FSSH. Green solid lines: NaF. Purple solid lines: SQC-TW. Red solid lines: NaF-TW. Converged results are obtained using three hundred discrete bath modes. For SQC-TW, the expression of the population–population correlation function is equivalent to that of ref 57 of Cotton and Miller, while eqs 10, 18, and 19 are used for the population–coherence correlation function because its SQC expression with triangle window functions of ref 57 is not exact for even the pure two-state system. More details of the parameters of the spin-boson models and the simulations are described in Section S3-A of the Supporting Information.

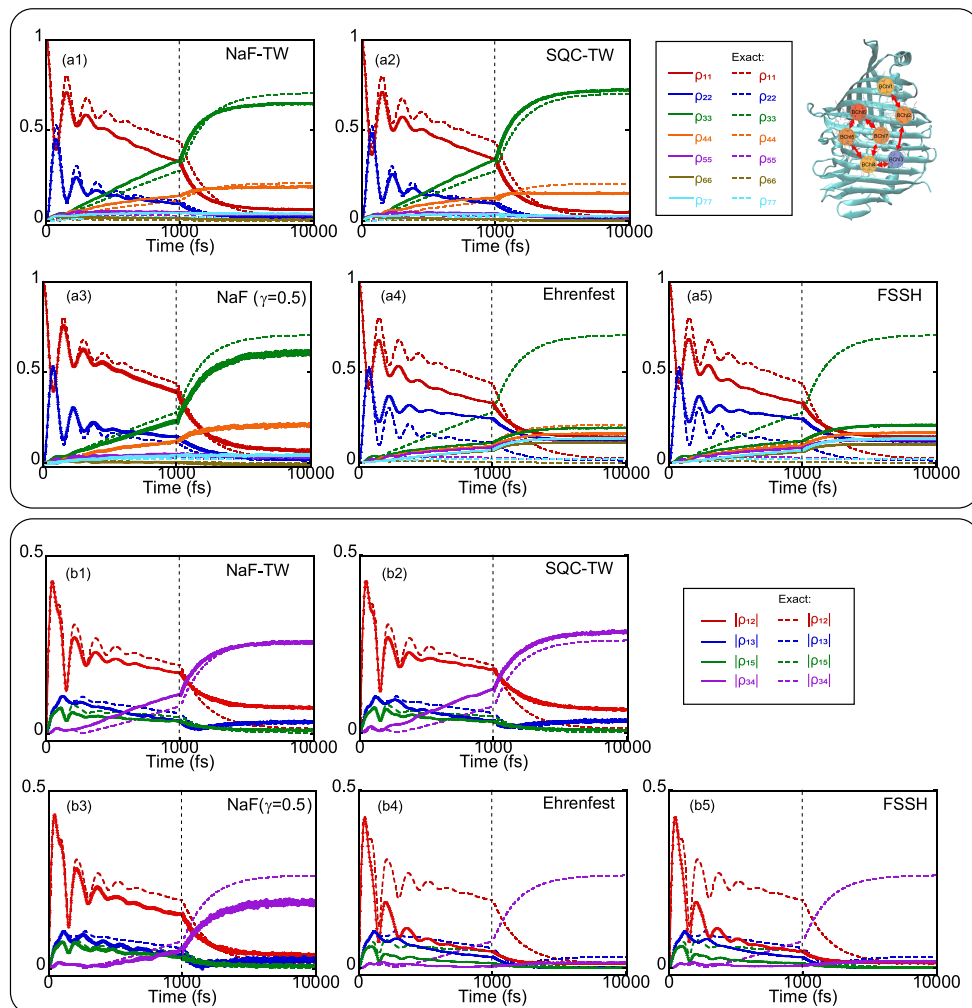


Figure 2. Initially occupied site is Site 1. Panel (a): The population dynamics of the seven-site FMO monomer model at temperature 77 K. The red, blue, green, orange, purple, brown, and cyan solid lines represent the population of Sites 1–7, respectively. Panel (b): Dynamics of the off-diagonal (coherence) terms of the reduced electronic density matrix of the same model. The red, blue, green, and purple solid lines illustrate $|\rho_{12}(t)|$, $|\rho_{13}(t)|$, $|\rho_{15}(t)|$, and $|\rho_{34}(t)|$, respectively. The exact results produced by HEOM are presented by dashed lines in corresponding colors. Subpanels (a1–a5) or Subpanels (b1–b5) denote the results of NaF-TW, SQC-TW, and NaF ($\gamma = 0.5$), Ehrenfest dynamics, and FSSH, respectively. One hundred discrete bath modes for each site are employed to obtain converged results. For SQC-TW, eqs 10, 18, and 19 are used for the population–coherence correlation function because its SQC expression with triangle window functions for the multistate system is not available in the literature. More details of the FMO model and the simulations are depicted in Section S3-A of the Supporting Information.

$\frac{\partial(-i\mathbf{d}^{(J)})}{\partial R_i} - \frac{\partial(-i\mathbf{d}^{(I)})}{\partial R_j} + i[-i\mathbf{d}^{(I)}, -i\mathbf{d}^{(J)}]_{\text{ele}}$ is close to zero such that we can construct the so-called quasi-diabatic basis.¹¹⁰ The null gauge field tensor indicates that the diabatic basis is strictly defined.^{88,110} E.g., it occurs when all adiabatic electronic states are involved, or when the adiabatic basis is parametrized along only a single DOF of the nuclear path.^{88,110} Because the diabatic basis is, in general, not well-defined, the gauge field tensor should be ignored with caution. Following the EOMs of NaF proposed in ref 104, the EOMs of NaF-TW similarly reads

$$\begin{aligned}\dot{\tilde{\mathbf{g}}}(\mathbf{R}) &= -iV^{(\text{eff})}(\mathbf{R}, \mathbf{P})\tilde{\mathbf{g}}(\mathbf{R}) \\ \dot{\mathbf{R}} &= \mathbf{M}^{-1}\mathbf{P} \\ \dot{\mathbf{P}} &= \mathbf{f}_{\text{nonadia}}(\mathbf{R}) - \nabla_{\mathbf{R}}E_{j_{\text{occ}}}(\mathbf{R})\end{aligned}\quad (24)$$

where $\tilde{\mathbf{g}}(\mathbf{R}) = \tilde{\mathbf{x}}(\mathbf{R}) + i\tilde{\mathbf{p}}(\mathbf{R})$, $(\tilde{\mathbf{x}}, \tilde{\mathbf{p}})$ are electronic mapping variables in the adiabatic representation, \mathbf{P} is the kinematic

nuclear momentum of the adiabatic representation^{55,86,88,104} (equivalently, the mapping diabatic momentum^{88,104}), the elements of the effective potential matrix, $\mathbf{V}^{(\text{eff})}$, are functions of nuclear phase space variables,

$$V_{nk}^{(\text{eff})}(\mathbf{R}, \mathbf{P}) = E_n(\mathbf{R})\delta_{nk} - i\mathbf{M}^{-1}\mathbf{P} \cdot \mathbf{d}_{nk}(\mathbf{R}) \quad (25)$$

and the nonadiabatic nuclear force reads

$$\mathbf{f}_{\text{nonadia}}(\mathbf{R}) = -\sum_{k \neq l} [(E_k(\mathbf{R}) - E_l(\mathbf{R}))\mathbf{d}_{lk}(\mathbf{R})]\tilde{\rho}_{kl}(\mathbf{R}) \quad (26)$$

In eq 26, $\tilde{\rho}_{kl}(\mathbf{R})$ is the element in the k -th row and l -th column of the matrix,

$$\tilde{\rho}(\mathbf{R}) = \frac{(1 + F/3)}{\text{Tr}_e[\tilde{\mathbf{g}}\tilde{\mathbf{g}}^\dagger]} \tilde{\mathbf{g}}\tilde{\mathbf{g}}^\dagger - \mathbf{1}/3 \quad (27)$$

The $1 + F/3$ term of eq 27 corresponds to the value of the so-called “zero-point energy parameter”, $1/3$, suggested in ref 54. (Please see more discussion in Section S4 of the Supporting

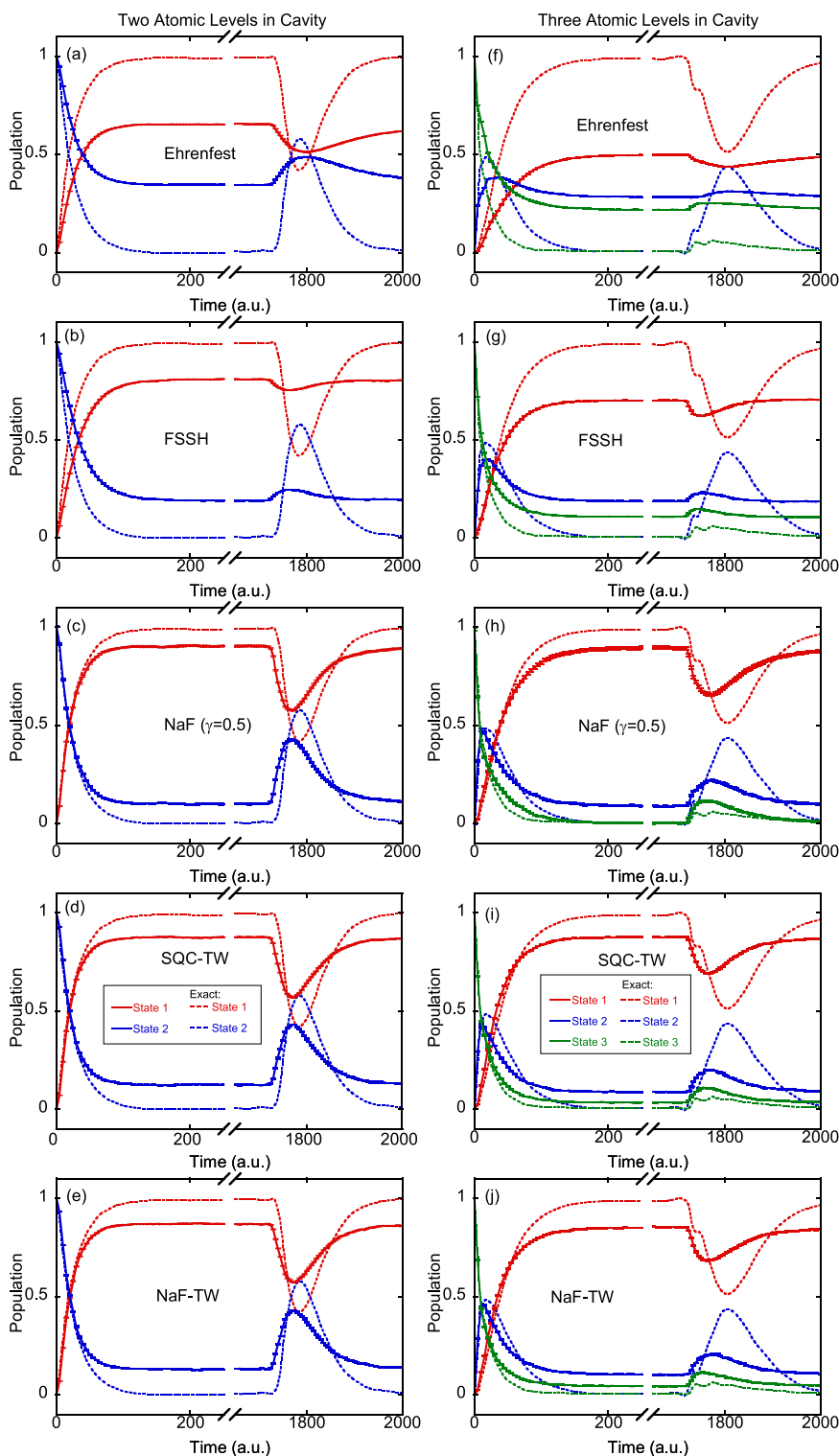


Figure 3. Panels (a–e): Results for the population dynamics of the two-level atom-in-cavity model. The red and blue solid lines represent the population of State 1 and that of State 2, respectively, while the dashed lines in corresponding colors demonstrate the exact results. Panels (f–j): Results of the population dynamics of the three-level atom-in-cavity model. The red, blue, and green solid lines represent the population of State 1, State 2, and State 3, respectively, while the dashed lines in corresponding colors demonstrate the exact results. Panels (a–e) or (f–j) present the results of Ehrenfest, FSSH, NaF ($\gamma = 0.5$), SQC-TW, and NaF-TW, respectively. The exact results are obtained from refs 129 and 130. Four hundred standing-wave modes for the optical field are used to obtain converged data. More details of the models and simulations are presented in Section S3-B of the Supporting Information.

Information.) The nonadiabatic nuclear force, eq 26, intrinsically accounts for nonadiabatic transition processes in the state-state coupling region and disappears in the region where

the state-state coupling vanishes. Its importance in the nuclear EOMs has been demonstrated by the applications to a few benchmark condensed phase model systems.¹⁰⁴ Following ref

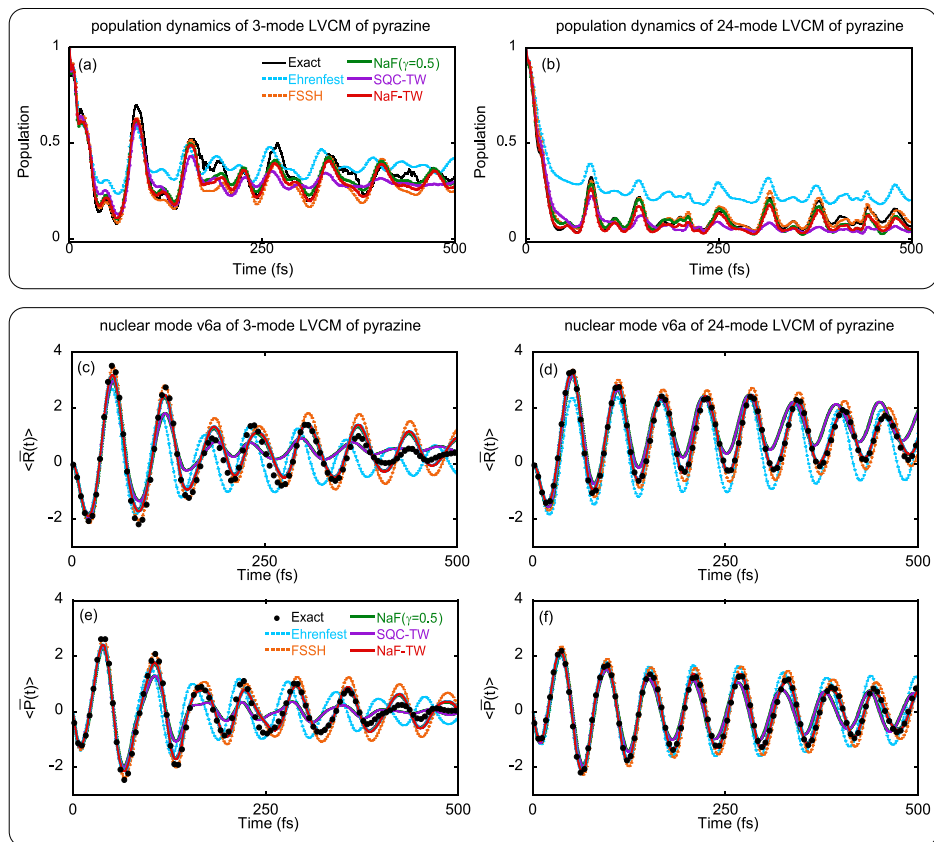


Figure 4. Panels (a,b) denote the population dynamics of the second state of the 2-state LVCM with 3 modes for the pyrazine molecule¹³¹ and that with 24 modes for the same molecule,¹³² respectively. Panels (c–f) denote the average coordinate and momentum of nuclear mode v_{6a} of the 3-mode and 24-mode LVCMs (for the pyrazine molecule), respectively. Cyan dashed lines: Ehrenfest dynamics. Orange dashed lines: FSSH. Green solid lines: NaF ($\gamma = 0.5$). Purple solid lines: SQC-TW. Red solid lines: NaF-TW. Black solid lines and black points represent exact results produced by the MCTDH package.¹³⁴

¹⁰⁴, the adiabatic nuclear force $-\nabla_{\mathbf{R}}E_{j_{\text{occ}}}(\mathbf{R})$ of eq 24 is contributed from the single-state adiabatic nuclear force that has the largest weight, i.e., $-\sum_k \nabla_{\mathbf{R}}E_k(\mathbf{R})\left(\prod_{j \neq k} h(\tilde{\rho}_{kk} - \tilde{\rho}_{jj})\right)$ with the Heaviside function $h(y) = \{1 \text{ if } y \geq 0 \text{ else } 0\}$. That is, the contribution of adiabatic force ingredients with smaller weights is neglected. We focus on this approach of the single-state adiabatic nuclear force from the dominant weight, although other approaches are also possible.¹⁰⁴ The NaF mapping energy in the adiabatic representation, $H_{\text{NaF}}(\mathbf{R}, \mathbf{P}, \tilde{\mathbf{x}}(\mathbf{R}), \tilde{\mathbf{p}}(\mathbf{R})) \equiv \frac{1}{2}\mathbf{P}^T \mathbf{M}^{-1} \mathbf{P} + E_{j_{\text{occ}}}(\mathbf{R})$, is conserved by rescaling the adiabatic kinematic nuclear momentum \mathbf{P} (that is equivalent to the mapping diabatic momentum^{88,104}) along the momentum vector after the integration of the EOMs of eq 24 as well as when the largest weight is switched.¹⁰⁴ If it is impossible to conserve the NaF energy when the largest weight is switched, the switching is prohibited, with no change of \mathbf{P} , and the single-state adiabatic nuclear force is still contributed by the gradient of the previously occupied adiabatic PES. The algorithm of NaF-TW is described in detail in **Section S2 of the Supporting Information**.

We consider a series of typical benchmark condensed phase and gas phase nonadiabatic model systems where numerically exact results are available, which have been used for testing the numerical performance of approximate dynamics methods in refs 86, 88, and 104. The latest SQC approach with triangle window functions of ref 57 (which is denoted as SQC-TW),

the conventional Ehrenfest dynamics,³⁷ the fewest-switches surface hopping (FSSH)¹⁶ algorithm described in ref 28, and the original NaF (with $\gamma = 1/2$) of ref 104 are also tested for comparison. The initial condition for nuclear DOFs is sampled from the Wigner distribution on nuclear coordinate-momentum phase space, which takes care of nuclear quantum effects in all the trajectory-based nonadiabatic dynamics methods for fair comparison. All simulations are performed in the adiabatic representation. When exact results are available in only the diabatic representation, the diabatic initial condition is transformed to its adiabatic counterpart, and dynamics results in the adiabatic representation are transformed back to the corresponding diabatic results.

We first consider standard system-bath models, where the system is bilinearly coupled with harmonic bath DOFs of a dissipative environment in the condensed phase. The coupling imparts a substantial influence from the bath environment and yields the reduced dynamics of the system across a broad spectrum ranging from coherent to dissipative regimes. Such models serve as pivotal tools for understanding important processes governing electron/exciton energy transfer dynamics in the realm of chemical and biological reactions. Methodologies that yield numerically exact results for condensed phase system-bath models, most in the diabatic representation, include quasi-adiabatic propagator path integral (QuAPI)^{111–113} and more efficient small matrix PI (SMat-PI),^{114,115} hierarchy equations of motion (HEOM),^{116–120} (multilayer) multiconfiguration time-dependent Hartree

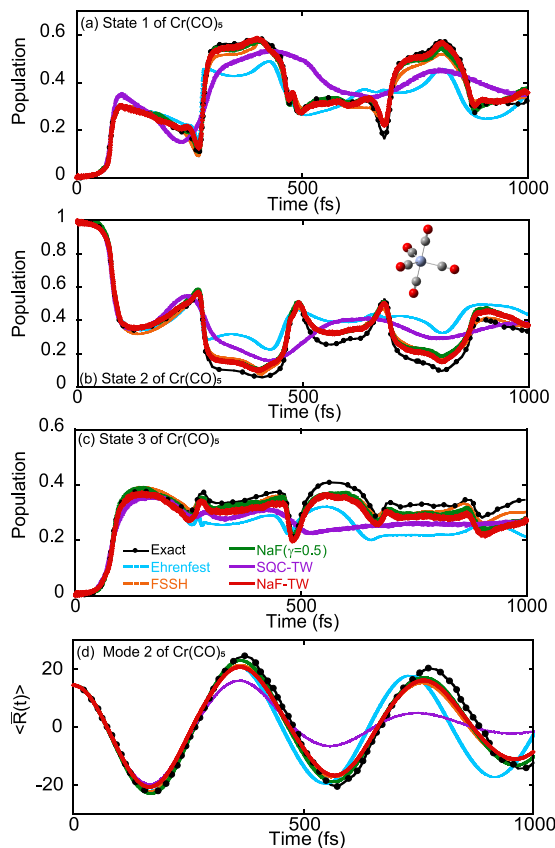


Figure 5. Panels (a–c) denote the population dynamics of States 1–3 of the 3-state 2-mode LVCM for the $\text{Cr}(\text{CO})_5$ molecule,¹³³ respectively. Panel (d) presents the expectation value of the coordinate variable of the second nuclear normal mode as a function of time. Cyan dashed lines: Ehrenfest dynamics. Orange dashed lines: FSSH. Green solid lines: NaF ($\gamma = 0.5$). Purple solid lines: SQC-TW. Red solid lines: NaF-TW. In Panels (a–d), black solid lines with black points denote exact data (obtained by MCTDH) from ref 133.

$[(\text{ML}-)\text{MCTDH}]$,^{121–123} time-dependent density matrix renormalization group (TD-DMRG),¹²⁴ and so forth. We use the two-site spin-boson model and the seven-site Fenna-Matthews-Olson (FMO) monomer model for testing trajectory-based nonadiabatic dynamics methods.

Figure 1 investigates four typical spin-boson models at low temperature, which range from weak to strong system-bath coupling. Three hundred discrete bath modes are utilized for the Ohmic spectral density. Initially, the (nuclear) bath DOFs are at thermal equilibrium and the system is in the diabatic excited state. (Please see more numerical details in **Section S3-A of the Supporting Information**.) In comparison to numerically exact data, while Ehrenfest dynamics produces the worst results, FSSH performs slightly better but does not capture the correct asymptotic behavior for a relatively long time. In contrast, SQC-TW, NaF, and NaF-TW yield results that are in overall good agreement with exact data. In addition, **Section S3-F of the Supporting Information** tests the two-state system-bath model for electron transfer reactions. Figure S4 (of the Supporting Information) illustrates that SQC-TW, NaF, and NaF-TW, using the CPS formulation or the CPS-TW representation that yields exact electronic dynamics of the pure two-state quantum system, noticeably outperform the original SQC method using square window functions of ref 125.

Figure 2 considers the seven-site FMO monomer model related to the photosynthetic organism of green sulfur bacteria. One hundred discrete bath modes per site are employed for the Debye spectral density. At time $t = 0$, the (nuclear) bath DOFs are at thermal equilibrium at 77 K and the first site is occupied. Both Ehrenfest dynamics and FSSH perform poorly even for relatively short time and fail to even qualitatively capture the steady-state behavior in the long-time limit. In comparison, SQC-TW, NaF, and NaF-TW show much better performance and are capable of reasonably describing the evolution of both electronic population and “coherence”, from the fast relaxation behavior at short time to the asymptotic behavior at long time.

We then consider two typical models of cavity quantum electrodynamics (cQED), where the matter system is tightly coupled to the vacuum field in a confined optical cavity.^{10,126–128} The first atom-in-cavity model involves two atomic energy levels, and the second one includes three energy levels. The highest energy level is initially occupied. More details of the models and initial conditions are described in **Supporting Information S2-B**. Figure 3 shows that both Ehrenfest dynamics and FSSH lead to significant deviation since a relatively short time and meet challenges in capturing the recoherence around $t = 1800$ au. In contrast, SQC-TW, NaF, and NaF-TW yield much more accurate data for the population dynamics of all energy levels and are capable of semiquantitatively describing the short time behavior, as well as the reabsorption and re-emission processes around $t = 1800$ au. The comparison between NaF and NaF-TW demonstrates that NaF dynamics performs robustly well, regardless of whether CPS or CPS-TW is used for the electronic representation. The results yielded by NaF-TW are close to those produced by the SQC-TW approach where independent mean-field trajectories are employed.

In all the three types of models above, the performance of NaF-TW is comparable to that of SQC-TW. Both NaF-TW and NaF outperform FSSH, which suggests that the NaF strategy is superior to conventional SH approaches in studying systems where the electronic states remain coupled all the time.

The third set of tests focuses on the linear vibronic coupling model (LVCM) that captures the characteristic of the pivotal conical intersection (CI) region of the molecular system in various photodriven phenomena. We use two LVCMs where MCTDH results in the diabatic representation are available. The first test case involves the two-electronic-state LVCM with three nuclear modes and that with 24 nuclear modes of refs 131 and 132 which mimic the S1/S2 conical intersection of the pyrazine molecule. The initial condition is set as the cross-product of the vibronic ground state and the excited electronically diabatic state (S2).^{131,132} The second test case employs a 3-electronic-state 2-nuclear-mode LVCM of the $\text{Cr}(\text{CO})_5$ molecule, where the initial condition is the cross-product of a Gaussian nuclear wave packet and the first excited electronically diabatic state as described in ref 133. More details of the LVCMs are demonstrated in **Section S3-C of the Supporting Information**. Figure 4 and Figure 5 show the results of the population dynamics in all these LVCM cases. FSSH, NaF, and NaF-TW significantly outperform Ehrenfest dynamics. While FSSH performs slightly better for the 2-state 24-mode case of pyrazine in Figure 4(b), NaF and NaF-TW are overall superior for the 2-state 3-mode case of pyrazine in Figure 4(a) as well as for the 3-state 2-mode LVCM of the

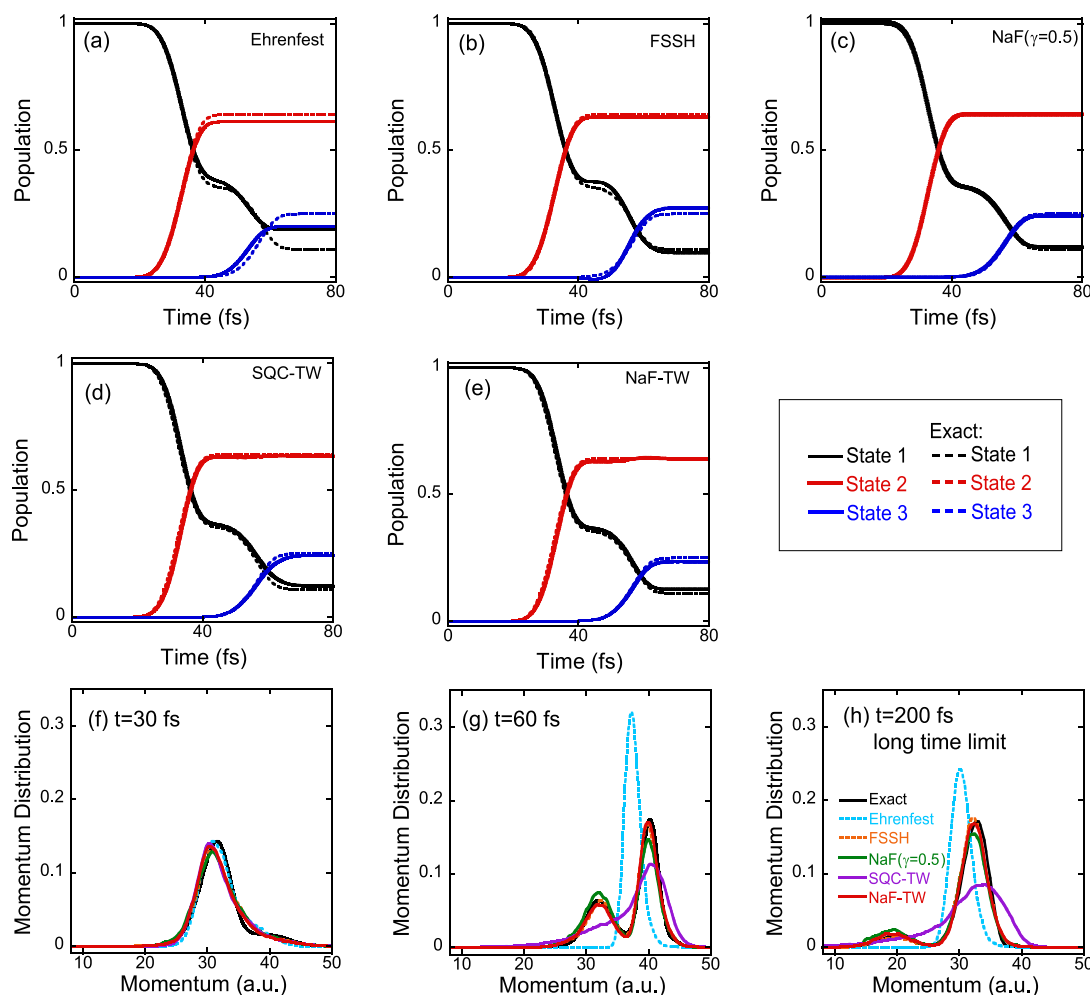


Figure 6. Panels (a–e) denote the population dynamics of the third photodissociation model of ref 46, where the black, red, and blue solid lines represent the population of States 1–3, respectively, and the exact results produced by DVR are presented by the dashed lines in corresponding colors. Panels (f–h) present the nuclear momentum distribution at $t = 30$, 60 , and 200 fs [which is in the asymptotic (long time) limit], respectively. The cyan dashed, orange dashed, green solid, purple solid, and red solid lines represent the results of Ehrenfest dynamics, FSSH, NaF ($\gamma = 0.5$), SQC-TW, and NaF-TW, respectively. The exact nuclear momentum distribution obtained by DVR is presented by the black solid line.

$\text{Cr}(\text{CO})_5$ molecule. NaF-TW considerably improves over SQC-TW for the peaks of long time dynamics of the pyrazine molecule in Figure 4(a,b) and for the population oscillation behavior when the evolution crosses or recrosses the CI region of the realistic gas phase $\text{Cr}(\text{CO})_5$ molecular system, as shown in Figure 5(a–c). NaF and NaF-TW also outperform SQC-TW and Ehrenfest dynamics in reproducing the expectation values of coordinate and momentum variables of the nuclear modes in LVCMs of the pyrazine molecule and the $\text{Cr}(\text{CO})_5$ molecule, as presented in Figure 4(c–f) and Figure 5(d), respectively. The results of nuclear dynamics generated by FSSH are comparable to those yielded by NaF and NaF-TW.

Finally, we test typical gas phase models with one anharmonic nuclear DOF where asymptotic regions are involved. The first case includes the coupled three-electronic-state photodissociation models of Miller and co-workers.⁴⁶ Numerical details are presented in Section S3-D of the Supporting Information. We focus on Model 3, which is the most challenging. Its nuclear momentum distribution in the long time limit produced by the numerically exact discrete variable representation (DVR) method¹³⁵ includes one peak in the higher momentum region and another one in the lower momentum region, while that yielded by Ehrenfest dynamics

has only one peak and entirely misses the two-peak characteristic in the asymptotic region. Figure 6 demonstrates the results of Model 3. Although SQC-TW noticeably outperforms Ehrenfest dynamics for the electronic population dynamics, it leads to a broader asymptotic nuclear momentum distribution with only one peak. This indicates that SQC-TW with mean field trajectories is not capable of semi-quantitatively capturing the two peaks in the nuclear momentum distribution in the long time limit, which is a consequence of the bifurcation nature of the nuclear motion in the asymptotic region where the nonadiabatic coupling vanishes. As shown in Figure 6, NaF-TW is superior to SQC-TW and yields results similar to those of FSSH and NaF, which are close to exact data by DVR. The second case involves Tully's standard scattering models,¹⁶ among which the extended coupling region (ECR) model is the most challenging one. More details are presented in Section S3-E of the Supporting Information. Quantum dynamics of the ECR model involves both the nuclear wavepacket that transmits forwardly and the one that reflects backwardly in asymptotic regions. The dramatic bifurcation characteristic has considerable influence on both electronic and nuclear dynamics. The performance of Ehrenfest dynamics is poor for the ECR model.

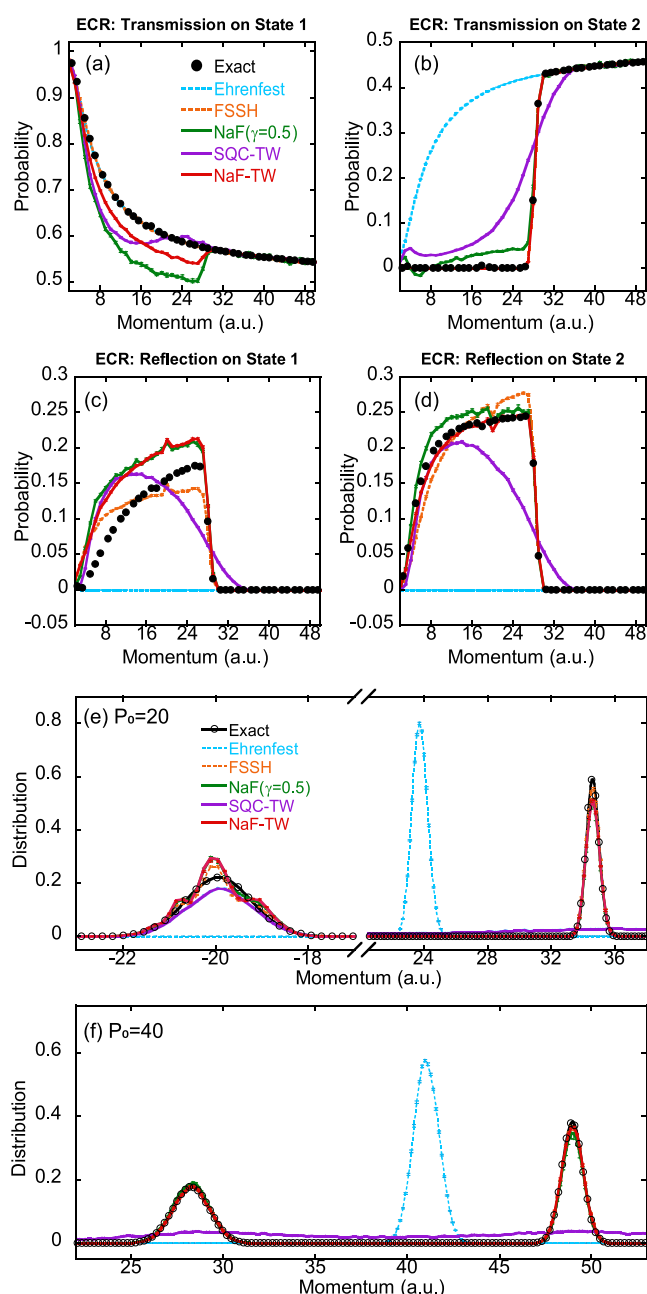


Figure 7. Panels (a,b) denote the transmission probability on (adiabatic) State 1 and that on State 2 for Tully's ECR model. Panels (c,d) denote the reflection probability on (adiabatic) State 1 and that on State 2 for the same model. Panels (e) and (f) present the asymptotic nuclear momentum distribution for the initial momentum $P_0 = 20$ of the center of the nuclear Gaussian wavepacket and that for $P_0 = 40$, respectively. Cyan dashed lines: Ehrenfest dynamics. Orange dashed lines: FSSH. Green solid lines: NaF ($\gamma = 0.5$). Purple solid lines: SQC-TW. Red solid lines: NaF-TW. Black points: Exact results by DVR.

Figure 7 shows that SQC-TW improves over Ehrenfest dynamics but is unable to reproduce the sharp step-like change in the transmission/reflection probability on State 2 as a function of the momentum of the center of the initial nuclear Gaussian wavepacket. In comparison, NaF-TW, as well as NaF and FSSH, leads to reasonably accurate electronic dynamics for the ECR model. **Figure 7(e)** and **Figure 7(f)** demonstrate that, while SQC-TW does not perform well in describing nuclear

dynamics for the ECR model in comparison to the exact DVR data, NaF-TW yields a much more accurate nuclear momentum distribution in the asymptotic region. Although NaF-TW and SQC-TW share the same CPS-TW expression of eq 21 for the electronic correlation function, the comparison in Figures 6 and 7 suggests that NaF dynamics (of NaF-TW) is more consistent than Ehrenfest-like dynamics (of SQC-TW) in describing the correct correlation between electronic and nuclear dynamics.

In comparison to the exact CPS formulation for discrete (electronic) DOFs, although the CPS-TW representation of the population–population correlation function (i.e., the population dynamics) is exact for only the pure two-state system,¹⁰³ its applications to three-state or multistate non-adiabatic systems (e.g., in Figures 2, 5, and 6) are also reasonably accurate in practice. As long as the phase space function of the initial total density operator (of both nuclear and electronic DOFs) is non-negative, the CPS-TW expression of the population dynamics (of electronic states) is guaranteed to be positive semidefinite, irrespective of the number of electronic states and the approximation of nuclear dynamics. The advantage of the CPS-TW representation helps NaF-TW outperform NaF in the cases of Figure 6(f–h) and Figure 7.

When the CPS-TW representation of electronic DOFs is used, in addition to NaF-TW, we show another variant that employs the commutator matrix as used in the original NaF approach,¹⁰⁴ which is denoted as NaF-TW2. As demonstrated by the extensive numerical tests in **Section S4 of the Supporting Information**, the numerical performance of NaF-TW2 is very similar to that of NaF-TW.¹⁰¹

In summary, since the unified phase space formulation with coordinate-momentum variables offers a powerful tool for studying composite systems, we use the triangle window functions^{54,57,58} and the $U(F)/U(F - 1)$ CPS^{82,84,85} to construct the CPS-TW representation for discrete (electronic) DOFs and employ it with the recently developed NaF strategy.¹⁰⁴ It leads to the NaF-TW approach for nonadiabatic transition dynamics. We test the performance of NaF-TW extensively for a series of standard benchmark condensed phase and gas phase nonadiabatic systems where numerically exact data are feasible for comparison. NaF-TW is able to capture the dynamical correlation between electronic and nuclear DOFs in a reasonably accurate manner. The performance of NaF-TW is similar to that of the SQC approach⁵⁷ in (molecular) systems where the electronic states remain coupled all the time. In addition, NaF-TW significantly outperforms the SQC approach in (molecular) systems where the evolution involves the asymptotic region where the state–state coupling disappears. While NaF-TW captures the correct correlation of electronic and nuclear dynamics in the asymptotic region, more advanced semiclassical methods^{50,73} beyond the SQC approach are necessary to accomplish the same task when independent mean field trajectories are used.

The comprehensive benchmark numerical tests in the main text as well as in the **Supporting Information** suggest that NaF dynamics is overall superior to conventional surface hopping dynamics and Ehrenfest-like dynamics in a broad region. Although the CPS formulation or CPS-TW representation may also be used with various surface hopping dynamics or Ehrenfest-like dynamics methods, NaF dynamics is highly recommended for its superiority. We also note that, since NaF or NaF-TW only involves the independent trajectory without the phase, it is rather difficult to perform well in the deep

quantum tunneling or quantum coherence region. The semiclassical-like approach or time-dependent multiconfiguration approach, which includes the NaF trajectory with its corresponding phase, will be a potential tool for studying the much more challenging quantum mechanical region.

Because the CPS formulation and CPS-TW representation can also be used for the interpretation of discrete quantum states of light atoms or those of high-frequency vibrational DOFs, the NaF strategy can be employed to study nuclear quantum effects in proton/hydrogen transfer processes.^{21,56,136} It is expected that further development of NaF-TW and the CPS formulations “in ever-increasing levels of abstraction”¹³⁷ will lead to a promising and robust trajectory-based approach for investigating electronically (and/or vibrationally) non-adiabatic transition phenomena (internal conversion, inter-system crossing, electron/hole/proton/hydrogen transfer, etc.) and dynamic processes with important quantum effects in complex/large composite systems in chemistry, biology, materials, environmental science, quantum information, quantum computation, and so forth.

ASSOCIATED CONTENT

Supporting Information

The Supporting Information is available free of charge at <https://pubs.acs.org/doi/10.1021/acs.jpcllett.4c00793>.

Five sections: proof that the CPS-TW expression of the time correlation function involving coherence terms is exact for electronic dynamics of the pure *F*-state quantum system; numerical details in evaluation of the time correlation function in NaF-TW, NaF, and SQC-TW; simulation details for models in the main text; comparison of different strategies employing triangle window functions; mapping triangle window functions onto constraint phase space leads to novel phase space formulations for the *F*-state quantum systems ([PDF](#))

AUTHOR INFORMATION

Corresponding Author

Jian Liu — Beijing National Laboratory for Molecular Sciences, Institute of Theoretical and Computational Chemistry, College of Chemistry and Molecular Engineering, Peking University, Beijing 100871, China;  orcid.org/0000-0002-2906-5858; Email: jianliupku@pku.edu.cn

Authors

Xin He — Beijing National Laboratory for Molecular Sciences, Institute of Theoretical and Computational Chemistry, College of Chemistry and Molecular Engineering, Peking University, Beijing 100871, China;  orcid.org/0000-0002-5189-7204

Xiangsong Cheng — Beijing National Laboratory for Molecular Sciences, Institute of Theoretical and Computational Chemistry, College of Chemistry and Molecular Engineering, Peking University, Beijing 100871, China;  orcid.org/0000-0001-8793-5092

Baihua Wu — Beijing National Laboratory for Molecular Sciences, Institute of Theoretical and Computational Chemistry, College of Chemistry and Molecular Engineering, Peking University, Beijing 100871, China;  orcid.org/0000-0002-1256-6859

Complete contact information is available at: <https://pubs.acs.org/doi/10.1021/acs.jpcllett.4c00793>

Notes

The authors declare no competing financial interest.

ACKNOWLEDGMENTS

This work was supported by the National Science Fund for Distinguished Young Scholars Grant No. 22225304. We acknowledge the High-performance Computing Platform of Peking University, Beijing PARATERA Tech Co., Ltd., and Guangzhou supercomputer center for providing computational resources. We thank Youhao Shang, Haocheng Lu, and Bingqi Li for useful discussions. We also thank Bill Miller for having encouraged us to investigate the window function approach.

REFERENCES

- (1) Polli, D.; Altoe, P.; Weingart, O.; Spillane, K. M.; Manzoni, C.; Brida, D.; Tomasello, G.; Orlandi, G.; Kukura, P.; Mathies, R. A.; et al. Conical Intersection Dynamics of the Primary Photoisomerization Event in Vision. *Nature* **2010**, *467*, 440–U88.
- (2) Martinez, T. J. Seaming Is Believing. *Nature* **2010**, *467*, 412–413.
- (3) Domcke, W.; Yarkony, D. R.; Köppel, H. *Conical Intersections: Theory, Computation and Experiment*; Advanced Series in Physical Chemistry, Vol. 17; World Scientific: Singapore, 2011; DOI: [10.1142/7803](https://doi.org/10.1142/7803).
- (4) Scholes, G. D.; Fleming, G. R.; Olaya-Castro, A.; van Grondelle, R. Lessons from Nature About Solar Light Harvesting. *Nat. Chem.* **2011**, *3*, 763–774.
- (5) Maiuri, M.; Ostroumov, E. E.; Saer, R. G.; Blankenship, R. E.; Scholes, G. D. Coherent Wavepackets in the Fenna-Matthews-Olson Complex Are Robust to Excitonic-Structure Perturbations Caused by Mutagenesis. *Nat. Chem.* **2018**, *10*, 177–183.
- (6) Smith, M. B.; Michl, J. Singlet Fission. *Chem. Rev.* **2010**, *110*, 6891–6936.
- (7) Scholes, G. D.; Rumbles, G. Excitons in Nanoscale Systems. *Nat. Mater.* **2006**, *5*, 683–696.
- (8) Long, R.; Prezhdo, O. V.; Fang, W.-H. Nonadiabatic Charge Dynamics in Novel Solar Cell Materials. *Wiley Interdiscip. Rev. Comput. Mol. Sci.* **2017**, *7*, No. e1305.
- (9) Wang, Y.-C.; Ke, Y.; Zhao, Y. The Hierarchical and Perturbative Forms of Stochastic Schrödinger Equations and Their Applications to Carrier Dynamics in Organic Materials. *Wiley Interdiscip. Rev. Comput. Mol. Sci.* **2019**, *9*, No. e1375.
- (10) Garcia-Vidal, F. J.; Ciuti, C.; Ebbesen, T. W. Manipulating Matter by Strong Coupling to Vacuum Fields. *Science* **2021**, *373*, No. eabd0336.
- (11) Mei, J.; Leung, N. L. C.; Kwok, R. T. K.; Lam, J. W. Y.; Tang, B. Z. Aggregation-Induced Emission: Together We Shine, United We Soar! *Chem. Rev.* **2015**, *115*, 11718–11940.
- (12) Ye, Z.; Lin, X.; Wang, N.; Zhou, J.; Zhu, M.; Qin, H.; Peng, X. Phonon-Assisted up-Conversion Photoluminescence of Quantum Dots. *Nat. Commun.* **2021**, *12*, 4283.
- (13) Xu, Y.; Liang, X.; Zhou, X.; Yuan, P.; Zhou, J.; Wang, C.; Li, B.; Hu, D.; Qiao, X.; Jiang, X.; et al. Highly Efficient Blue Fluorescent Oleds Based on Upper Level Triplet–Singlet Intersystem Crossing. *Adv. Mater.* **2019**, *31*, No. 1807388.
- (14) Hammes-Schiffer, S. Theoretical Perspectives on Non-Born-Oppenheimer Effects in Chemistry. *Philos. Trans. Royal Soc. A* **2022**, *380*, 20200377.
- (15) Tully, J. C.; Preston, R. K. Trajectory Surface Hopping Approach to Nonadiabatic Molecular Collisions: The Reaction of H+ with D2. *J. Chem. Phys.* **1971**, *55*, 562–572.
- (16) Tully, J. C. Molecular Dynamics with Electronic Transitions. *J. Chem. Phys.* **1990**, *93*, 1061–1071.
- (17) Bjerre, A.; Nikitin, E. E. Energy Transfer in Collisions of an Excited Sodium Atom with a Nitrogen Molecule. *Chem. Phys. Lett.* **1967**, *1*, 179–181.

- (18) Nikitin, E. E. *The Theory of Nonadiabatic Transitions: Recent Development with Exponential Models*; Advances in Quantum Chemistry, Vol. 5; Academic Press, Inc.: New York, 1970; pp 135–184; DOI: 10.1016/S0065-3276(08)60338-X.
- (19) Duren, R. Differential Cross Sections for Alkali-Halogen Collisions from Trajectory Calculations on Intersecting Surfaces. *J. Phys. B: At. Mol. Opt. Phys.* **1973**, *6*, 1801–1813.
- (20) Blais, N. C.; Truhlar, D. G. Trajectory-Surface-Hopping Study of $\text{Na}(3p^2P) + \text{H}_2 \rightarrow \text{Na}(3s^2S) + \text{H}_2(v', J', \theta)$. *J. Chem. Phys.* **1983**, *79*, 1334–1342.
- (21) Hammes-Schiffer, S.; Tully, J. C. Proton Transfer in Solution: Molecular Dynamics with Quantum Transitions. *J. Chem. Phys.* **1994**, *101*, 4657–4667.
- (22) Zhu, C. Y.; Nobusada, K.; Nakamura, H. New Implementation of the Trajectory Surface Hopping Method with Use of the Zhu-Nakamura Theory. *J. Chem. Phys.* **2001**, *115*, 3031–3044.
- (23) Craig, C. F.; Duncan, W. R.; Prezhdo, O. V. Trajectory Surface Hopping in the Time-Dependent Kohn-Sham Approach for Electron-Nuclear Dynamics. *Phys. Rev. Lett.* **2005**, *95*, No. 163001.
- (24) Granucci, G.; Persico, M. Critical Appraisal of the Fewest Switches Algorithm for Surface Hopping. *J. Chem. Phys.* **2007**, *126*, 134114.
- (25) Shenvi, N.; Subotnik, J. E.; Yang, W. Phase-Corrected Surface Hopping: Correcting the Phase Evolution of the Electronic Wavefunction. *J. Chem. Phys.* **2011**, *135*, No. 024101.
- (26) Jaeger, H. M.; Fischer, S.; Prezhdo, O. V. Decoherence-Induced Surface Hopping. *J. Chem. Phys.* **2012**, *137*, 22A545.
- (27) Wang, L.; Akimov, A.; Prezhdo, O. V. Recent Progress in Surface Hopping: 2011–2015. *J. Phys. Chem. Lett.* **2016**, *7*, 2100–2112.
- (28) Peng, J.; Xie, Y.; Hu, D.; Du, L.; Lan, Z. Treatment of Nonadiabatic Dynamics by on-the-Fly Trajectory Surface Hopping Dynamics. *Acta Phys.-Chim. Sin.* **2019**, *35*, 28–48.
- (29) Barbatti, M. Nonadiabatic Dynamics with Trajectory Surface Hopping Method. *Wiley Interdiscip. Rev. Comput. Mol. Sci.* **2011**, *1*, 620–633.
- (30) Tully, J. C. Perspective: Nonadiabatic Dynamics Theory. *J. Chem. Phys.* **2012**, *137*, 22A301.
- (31) Granucci, G.; Persico, M.; Spighi, G. Surface Hopping Trajectory Simulations with Spin-Orbit and Dynamical Couplings. *J. Chem. Phys.* **2012**, *137*, 22A501.
- (32) Cui, G.; Thiel, W. Generalized Trajectory Surface-Hopping Method for Internal Conversion and Intersystem Crossing. *J. Chem. Phys.* **2014**, *141*, 124101.
- (33) Mai, S.; Marquetand, P.; Gonzalez, L. A General Method to Describe Intersystem Crossing Dynamics in Trajectory Surface Hopping. *Int. J. Quantum Chem.* **2015**, *115*, 1215–1231.
- (34) Subotnik, J. E.; Jain, A.; Landry, B.; Petit, A.; Ouyang, W.; Bellonzi, N. Understanding the Surface Hopping View of Electronic Transitions and Decoherence. *Annu. Rev. Phys. Chem.* **2016**, *67*, 387–417.
- (35) Martens, C. C. Surface Hopping by Consensus. *J. Phys. Chem. Lett.* **2016**, *7*, 2610–2615.
- (36) Kapral, R. Surface Hopping from the Perspective of Quantum-Classical Liouville Dynamics. *Chem. Phys.* **2016**, *481*, 77–83.
- (37) Ehrenfest, P. Bemerkung Über Die Angenäherte Gültigkeit Der Klassischen Mechanik Innerhalb Der Quantenmechanik. *Z. Phys.* **1927**, *45*, 455–457.
- (38) Delos, J. B.; Thorson, W. R.; Knudson, S. K. Semiclassical Theory of Inelastic Collisions. I. Classical Picture and Semiclassical Formulation. *Phys. Rev. A* **1972**, *6*, 709–720.
- (39) Billing, G. D. On the Applicability of the Classical Trajectory Equations in Inelastic Scattering Theory. *Chem. Phys. Lett.* **1975**, *30*, 391–393.
- (40) Micha, D. A. A Self-Consistent Eikonal Treatment of Electronic Transitions in Molecular Collisions. *J. Chem. Phys.* **1983**, *78*, 7138–7145.
- (41) Miller, W.; McCurdy, C. Classical Trajectory Model for Electronically Nonadiabatic Collision Phenomena. A Classical Analog for Electronic Degrees of Freedom. *J. Chem. Phys.* **1978**, *69*, 5163–5173.
- (42) Meyer, H.-D.; Miller, W. H. A Classical Analog for Electronic Degrees of Freedom in Nonadiabatic Collision Processes. *J. Chem. Phys.* **1979**, *70*, 3214–3223.
- (43) Sun, X.; Wang, H.; Miller, W. H. Semiclassical Theory of Electronically Nonadiabatic Dynamics: Results of a Linearized Approximation to the Initial Value Representation. *J. Chem. Phys.* **1998**, *109*, 7064–7074.
- (44) Wang, H.; Song, X.; Chandler, D.; Miller, W. H. Semiclassical Study of Electronically Nonadiabatic Dynamics in the Condensed-Phase: Spin-Boson Problem with Debye Spectral Density. *J. Chem. Phys.* **1999**, *110*, 4828–4840.
- (45) Stock, G.; Muller, U. Flow of Zero-Point Energy and Exploration of Phase Space in Classical Simulations of Quantum Relaxation Dynamics. *J. Chem. Phys.* **1999**, *111*, 65–76.
- (46) Coronado, E. A.; Xing, J.; Miller, W. H. Ultrafast Non-Adiabatic Dynamics of Systems with Multiple Surface Crossings: A Test of the Meyer-Miller Hamiltonian with Semiclassical Initial Value Representation Methods. *Chem. Phys. Lett.* **2001**, *349*, 521–529.
- (47) Golosov, A. A.; Reichman, D. R. Classical Mapping Approaches for Nonadiabatic Dynamics: Short Time Analysis. *J. Chem. Phys.* **2001**, *114*, 1065–1074.
- (48) Bonella, S.; Montemayor, D.; Coker, D. F. Linearized Path Integral Approach for Calculating Nonadiabatic Time Correlation Functions. *Proc. Natl. Acad. Sci. U. S. A.* **2005**, *102*, 6715–6719.
- (49) Stock, G.; Thoss, M. Classical Description of Nonadiabatic Quantum Dynamics. In *Advances in Chemical Physics*; Advances in Chemical Physics Vol. 131; Rice, S. A., Ed.; John Wiley and Sons, Inc.: Hoboken, NJ, 2005; pp 243–375; DOI: 10.1002/0471739464.ch5.
- (50) Ananth, N.; Venkataraman, C.; Miller, W. H. Semiclassical Description of Electronically Nonadiabatic Dynamics Via the Initial Value Representation. *J. Chem. Phys.* **2007**, *127*, No. 084114.
- (51) Tao, G.; Miller, W. H. Semiclassical Description of Electronic Excitation Population Transfer in a Model Photosynthetic System. *J. Phys. Chem. Lett.* **2010**, *1*, 891–894.
- (52) Huo, P.; Miller, T. F.; Coker, D. F. Communication: Predictive Partial Linearized Path Integral Simulation of Condensed Phase Electron Transfer Dynamics. *J. Chem. Phys.* **2013**, *139*, 151103.
- (53) Cotton, S. J.; Miller, W. H. Symmetrical Windowing for Quantum States in Quasi-Classical Trajectory Simulations: Application to Electronically Non-Adiabatic Processes. *J. Chem. Phys.* **2013**, *139*, 234112.
- (54) Cotton, S. J.; Miller, W. H. A New Symmetrical Quasi-Classical Model for Electronically Non-Adiabatic Processes: Application to the Case of Weak Non-Adiabatic Coupling. *J. Chem. Phys.* **2016**, *145*, 144108.
- (55) Cotton, S. J.; Liang, R.; Miller, W. H. On the Adiabatic Representation of Meyer-Miller Electronic-Nuclear Dynamics. *J. Chem. Phys.* **2017**, *147*, No. 064112.
- (56) Kananenka, A. A.; Hsieh, C. Y.; Cao, J. S.; Geva, E. Nonadiabatic Dynamics Via the Symmetrical Quasi-Classical Method in the Presence of Anharmonicity. *J. Phys. Chem. Lett.* **2018**, *9*, 319–326.
- (57) Cotton, S. J.; Miller, W. H. Trajectory-Adjusted Electronic Zero Point Energy in Classical Meyer-Miller Vibronic Dynamics: Symmetrical Quasiclassical Application to Photodissociation. *J. Chem. Phys.* **2019**, *150*, 194110.
- (58) Cotton, S. J.; Miller, W. H. A Symmetrical Quasi-Classical Windowing Model for the Molecular Dynamics Treatment of Non-Adiabatic Processes Involving Many Electronic States. *J. Chem. Phys.* **2019**, *150*, 104101.
- (59) Saller, M. A. C.; Kelly, A.; Richardson, J. O. On the Identity of the Identity Operator in Nonadiabatic Linearized Semiclassical Dynamics. *J. Chem. Phys.* **2019**, *150*, No. 071101.
- (60) Gao, X.; Saller, M. A. C.; Liu, Y.; Kelly, A.; Richardson, J. O.; Geva, E. Benchmarking Quasiclassical Mapping Hamiltonian

- Methods for Simulating Electronically Nonadiabatic Molecular Dynamics. *J. Chem. Theory. Comput.* **2020**, *16*, 2883–2895.
- (61) Runeson, J. E.; Richardson, J. O. Generalized Spin Mapping for Quantum-Classical Dynamics. *J. Chem. Phys.* **2020**, *152*, No. 084110.
- (62) Saller, M. A. C.; Kelly, A.; Geva, E. Benchmarking Quasiclassical Mapping Hamiltonian Methods for Simulating Cavity-Modified Molecular Dynamics. *J. Phys. Chem. Lett.* **2021**, *12*, 3163–3170.
- (63) Stock, G.; Thoss, M. Semiclassical Description of Nonadiabatic Quantum Dynamics. *Phys. Rev. Lett.* **1997**, *78*, 578–581.
- (64) Liang, R.; Cotton, S. J.; Binder, R.; Hegger, R.; Burghardt, I.; Miller, W. H. The Symmetrical Quasi-Classical Approach to Electronically Nonadiabatic Dynamics Applied to Ultrafast Exciton Migration Processes in Semiconducting Polymers. *J. Chem. Phys.* **2018**, *149*, No. 044101.
- (65) Tang, D.; Fang, W.-H.; Shen, L.; Cui, G. Combining Meyer-Miller Hamiltonian with Electronic Structure Methods for on-the-Fly Nonadiabatic Dynamics Simulations: Implementation and Application. *Phys. Chem. Chem. Phys.* **2019**, *21*, 17109–17117.
- (66) Peng, J.; Xie, Y.; Hu, D.; Lan, Z. Analysis of Bath Motion in MM-SQC Dynamics Via Dimensionality Reduction Approach: Principal Component Analysis. *J. Chem. Phys.* **2021**, *154*, No. 094122.
- (67) Hu, D.; Xie, Y.; Peng, J.; Lan, Z. On-the-Fly Symmetrical Quasi-Classical Dynamics with Meyer–Miller Mapping Hamiltonian for the Treatment of Nonadiabatic Dynamics at Conical Intersections. *J. Chem. Theory. Comput.* **2021**, *17*, 3267–3279.
- (68) Zheng, J.; Peng, J.; Xie, Y.; Long, Y.; Ning, X.; Lan, Z. Study of the Exciton Dynamics in Perylene Bisimide (PBI) Aggregates with Symmetrical Quasiclassical Dynamics Based on the Meyer-Miller Mapping Hamiltonian. *Phys. Chem. Chem. Phys.* **2020**, *22*, 18192–18204.
- (69) Zheng, J.; Xie, Y.; Jiang, S.; Long, Y.; Ning, X.; Lan, Z. Initial Sampling in Symmetrical Quasiclassical Dynamics Based on Li-Miller Mapping Hamiltonian. *Phys. Chem. Chem. Phys.* **2019**, *21*, 26502–26514.
- (70) Xie, Y.; Zheng, J.; Lan, Z. Performance Evaluation of the Symmetrical Quasi-Classical Dynamics Method Based on Meyer-Miller Mapping Hamiltonian in the Treatment of Site-Exciton Models. *J. Chem. Phys.* **2018**, *149*, 174105.
- (71) Hu, Z.; Sun, X. All-Atom Nonadiabatic Semiclassical Mapping Dynamics for Photoinduced Charge Transfer of Organic Photovoltaic Molecules in Explicit Solvents. *J. Chem. Theory. Comput.* **2022**, *18*, 5819–5836.
- (72) Liu, Y.; Gao, X.; Lai, Y.; Mulvihill, E.; Geva, E. Electronic Dynamics through Conical Intersections Via Quasiclassical Mapping Hamiltonian Methods. *J. Chem. Theory. Comput.* **2020**, *16*, 4479–4488.
- (73) Miller, W. H. Electronically Nonadiabatic Dynamics Via Semiclassical Initial Value Methods. *J. Phys. Chem. A* **2009**, *113*, 1405–1415.
- (74) Miller, W. H. Spiers Memorial Lecture - Quantum and Semiclassical Theory of Chemical Reaction Rates. *Faraday Discuss.* **1998**, *110*, 1–21.
- (75) Sun, X.; Miller, W. H. Forward-Backward Initial Value Representation for Semiclassical Time Correlation Functions. *J. Chem. Phys.* **1999**, *110*, 6635–6644.
- (76) Miller, W. H. Quantum Dynamics of Complex Molecular Systems. *Proc. Natl. Acad. Sci. U. S. A.* **2005**, *102*, 6660–6664.
- (77) Truhlar, D. G. Effective Potentials for Intermediate-Energy Electron Scattering: Testing Theoretical Models. In *Chemical Applications of Atomic and Molecular Electrostatic Potentials*; Politzer, P., Truhlar, D. G., Eds.; Springer US: Boston, MA, 1981; pp 123–172; DOI: [10.1007/978-1-4757-9634-6_8](https://doi.org/10.1007/978-1-4757-9634-6_8).
- (78) Zhu, C. Y.; Jasper, A. W.; Truhlar, D. G. Non-Born-Oppenheimer Trajectories with Self-Consistent Decay of Mixing. *J. Chem. Phys.* **2004**, *120*, 5543–5557.
- (79) Zhu, C. Y.; Nangia, S.; Jasper, A. W.; Truhlar, D. G. Coherent Switching with Decay of Mixing: An Improved Treatment of Electronic Coherence for Non-Born-Oppenheimer Trajectories. *J. Chem. Phys.* **2004**, *121*, 7658–7670.
- (80) Yonehara, T.; Takatsuka, K. Phase-Space Averaging and Natural Branching of Nuclear Paths for Nonadiabatic Electron Wavepacket Dynamics. *J. Chem. Phys.* **2008**, *129*, 134109.
- (81) Tao, G. Coherence-Controlled Nonadiabatic Dynamics Via State-Space Decomposition: A Consistent Way to Incorporate Ehrenfest and Born-Oppenheimer-Like Treatments of Nuclear Motion. *J. Phys. Chem. Lett.* **2016**, *7*, 4335–4339.
- (82) Liu, J. A Unified Theoretical Framework for Mapping Models for the Multi-State Hamiltonian. *J. Chem. Phys.* **2016**, *145*, 204105.
- (83) Liu, J. Isomorphism between the Multi-State Hamiltonian and the Second-Quantized Many-Electron Hamiltonian with Only 1-Electron Interactions. *J. Chem. Phys.* **2017**, *146*, No. 024110.
- (84) He, X.; Liu, J. A New Perspective for Nonadiabatic Dynamics with Phase Space Mapping Models. *J. Chem. Phys.* **2019**, *151*, No. 024105.
- (85) He, X.; Gong, Z.; Wu, B.; Liu, J. Negative Zero-Point-Energy Parameter in the Meyer-Miller Mapping Model for Nonadiabatic Dynamics. *J. Phys. Chem. Lett.* **2021**, *12*, 2496–2501.
- (86) He, X.; Wu, B.; Gong, Z.; Liu, J. Commutator Matrix in Phase Space Mapping Models for Nonadiabatic Quantum Dynamics. *J. Phys. Chem. A* **2021**, *125*, 6845–6863.
- (87) Liu, J.; He, X.; Wu, B. Unified Formulation of Phase Space Mapping Approaches for Nonadiabatic Quantum Dynamics. *Acc. Chem. Res.* **2021**, *54*, 4215–4228.
- (88) He, X.; Wu, B.; Shang, Y.; Li, B.; Cheng, X.; Liu, J. New Phase Space Formulations and Quantum Dynamics Approaches. *Wiley Interdiscip. Rev. Comput. Mol. Sci.* **2022**, *12*, No. e1619.
- (89) Wu, B.; He, X.; Liu, J. Phase Space Mapping Theory for Nonadiabatic Quantum Molecular Dynamics. In *Time-Dependent Density Functional Theory: Nonadiabatic Molecular Dynamics*; Zhu, C., Ed.; Jenny Stanford Publishing: New York, 2022; DOI: [10.1201/9781003319214-11](https://doi.org/10.1201/9781003319214-11).
- (90) Gardner, J.; Douglas-Gallardo, O. A.; Stark, W. G.; Westermayr, J.; Janke, S. M.; Habershon, S.; Maurer, R. J. Nqdynamics.Jl: A Julia Package for Nonadiabatic Quantum Classical Molecular Dynamics in the Condensed Phase. *J. Chem. Phys.* **2022**, *156*, 174801.
- (91) Nakahara, M. *Geometry, Topology, and Physics*, 2 ed.; Institute of Physics Publishing: Bristol, 2003; DOI: [10.1201/9781315275826](https://doi.org/10.1201/9781315275826).
- (92) Atiyah, M. F.; Todd, J. A. On Complex Stiefel Manifolds. *Math. Proc. Cambridge Philos. Soc.* **1960**, *56*, 342–353.
- (93) Shang, Y.; Cheng, X.; Liu, J. Manuscript to be submitted.
- (94) Stratonovich, R. L. On Distributions in Representation Space. *Zh. Eksp. Teor. Fiz.* **1956**, *31*, 1012.
- (95) Berezin, F. A. General Concept of Quantization. *Commun. Math. Phys.* **1975**, *40*, 153–174.
- (96) Klimov, A. B. Exact Evolution Equations for SU(2) Quasidistribution Functions. *J. Math. Phys.* **2002**, *43*, 2202–2213.
- (97) Tilma, T.; Nemoto, K. SU(N)-Symmetric Quasi-Probability Distribution Functions. *J. Phys. A: Math. Theor.* **2012**, *45*, No. 015302.
- (98) Bargueño, P.; Miret-Artés, S. Dissipative and Stochastic Geometric Phase of a Qubit within a Canonical Langevin Framework. *Phys. Rev. A* **2013**, *87*, No. 012125.
- (99) Peñate-Rodríguez, H. C.; Dorta-Urra, A.; Bargueño, P.; Rojas-Lorenzo, G.; Miret-Artés, S. A Langevin Canonical Approach to the Dynamics of Chiral Systems: Populations and Coherences. *Chirality* **2013**, *25*, 514–520.
- (100) Peñate-Rodríguez, H. C.; Dorta-Urra, A.; Bargueño, P.; Rojas-Lorenzo, G.; Miret-Artés, S. A Langevin Canonical Approach to the Dynamics of Chiral Systems: Thermal Averages and Heat Capacity. *Chirality* **2014**, *26*, 319–325.
- (101) Luis, A.; García, G. Semiclassical Approaches Are Inconsistent. arXiv.1801.03642 **2018**, DOI: [10.48550/arXiv.1801.03642](https://arxiv.org/abs/1801.03642).
- (102) García, G.; Ares, L.; Luis, A. Phase Space Quantum-Classical Hybrid Model. *Ann. Phys.* **2019**, *411*, No. 167961.
- (103) Cheng, X.; He, X.; Liu, J. A Novel Class of Phase Space Representations for the Exact Population Dynamics of Two-State

- Quantum Systems and the Relation to Symmetrical Window Functions. *Chin. J. Chem. Phys.* **2024**, *37*, 230–254.
- (104) Wu, B.; He, X.; Liu, J. Nonadiabatic Field on Quantum Phase Space: A Century after Ehrenfest. *J. Phys. Chem. Lett.* **2024**, *15*, 644–658.
- (105) Lang, H.; Vendrell, O.; Hauke, P. Generalized Discrete Truncated Wigner Approximation for Nonadiabatic Quantum-Classical Dynamics. *J. Chem. Phys.* **2021**, *155*, No. 024111.
- (106) Shang, Y. On Quantum Phase Space Mapping Theory and Trajectory-Based Dynamics Approaches. *B.S. Thesis, Undergraduate*; Liu, J., Advisor; Peking University, China, 2022.
- (107) Miller, W. H.; Cotton, S. J. Communication: Wigner Functions in Action-Angle Variables, Bohr-Sommerfeld Quantization, the Heisenberg Correspondence Principle, and a Symmetrical Quasi-Classical Approach to the Full Electronic Density Matrix. *J. Chem. Phys.* **2016**, *145*, No. 081102.
- (108) Lang, H. Quantum Dynamics of Chemical Systems with Large Number of Degrees of Freedom: Linearized Phase Space Methods and Quantum Simulations. *Ph.D. Dissertation*; Hauke, P. H. J., Romagosa, O. V., Advisors; Ruprecht Karl University of Heidelberg: Heidelberg, Baden-Württemberg, Germany, 2022.
- (109) Das, A. *Field Theory: A Path Integral Approach*; World Scientific: Singapore, 2019; DOI: [10.1142/11339](https://doi.org/10.1142/11339).
- (110) Domcke, W.; Yarkony, D.; Köppel, H. *Conical Intersections: Electronic Structure, Dynamics & Spectroscopy*; World Scientific: Singapore, 2004; DOI: [10.1142/5406](https://doi.org/10.1142/5406).
- (111) Makarov, D. E.; Makri, N. Path Integrals for Dissipative Systems by Tensor Multiplication. Condensed Phase Quantum Dynamics for Arbitrarily Long Time. *Chem. Phys. Lett.* **1994**, *221*, 482–491.
- (112) Makri, N.; Makarov, D. E. Tensor Propagator for Iterative Quantum Time Evolution of Reduced Density Matrices. II. Numerical Methodology. *J. Chem. Phys.* **1995**, *102*, 4611–4618.
- (113) Makri, N.; Makarov, D. E. Tensor Propagator for Iterative Quantum Time Evolution of Reduced Density Matrices. I. Theory. *J. Chem. Phys.* **1995**, *102*, 4600–4610.
- (114) Makri, N. Small Matrix Path Integral with Extended Memory. *J. Chem. Theory Comput.* **2021**, *17*, 1–6.
- (115) Makri, N. Small Matrix Disentanglement of the Path Integral: Overcoming the Exponential Tensor Scaling with Memory Length. *J. Chem. Phys.* **2020**, *152*, No. 041104.
- (116) Tanimura, Y.; Kubo, R. Time Evolution of a Quantum System in Contact with a Nearly Gaussian-Markoffian Noise Bath. *J. Phys. Soc. Jpn.* **1989**, *58*, 101–114.
- (117) Yan, Y.-A.; Yang, F.; Liu, Y.; Shao, J. Hierarchical Approach Based on Stochastic Decoupling to Dissipative Systems. *Chem. Phys. Lett.* **2004**, *395*, 216–221.
- (118) Xu, R.-X.; Cui, P.; Li, X.-Q.; Mo, Y.; Yan, Y. Exact Quantum Master Equation Via the Calculus on Path Integrals. *J. Chem. Phys.* **2005**, *122*, No. 041103.
- (119) Shao, J. Stochastic Description of Quantum Open Systems: Formal Solution and Strong Dissipation Limit. *Chem. Phys.* **2006**, *322*, 187–192.
- (120) Moix, J. M.; Cao, J. A Hybrid Stochastic Hierarchy Equations of Motion Approach to Treat the Low Temperature Dynamics of Non-Markovian Open Quantum Systems. *J. Chem. Phys.* **2013**, *139*, 134106.
- (121) Meyer, H.-D.; Manthe, U.; Cederbaum, L. S. The Multi-Configurational Time-Dependent Hartree Approach. *Chem. Phys. Lett.* **1990**, *165*, 73–78.
- (122) Thoss, M.; Wang, H.; Miller, W. H. Self-Consistent Hybrid Approach for Complex Systems: Application to the Spin-Boson Model with Debye Spectral Density. *J. Chem. Phys.* **2001**, *115*, 2991–3005.
- (123) Wang, H.; Thoss, M. Multilayer Formulation of the Multiconfiguration Time-Dependent Hartree Theory. *J. Chem. Phys.* **2003**, *119*, 1289–1299.
- (124) Ren, J. J.; Li, W. T.; Jiang, T.; Wang, Y. H.; Shuai, Z. G. Time-Dependent Density Matrix Renormalization Group Method for Quantum Dynamics in Complex Systems. *Wiley Interdiscip. Rev. Comput. Mol. Sci.* **2022**, *12*, No. e1614.
- (125) Cotton, S. J.; Igumenshchev, K.; Miller, W. H. Symmetrical Windowing for Quantum States in Quasi-Classical Trajectory Simulations: Application to Electron Transfer. *J. Chem. Phys.* **2014**, *141*, No. 084104.
- (126) Haugland, T. S.; Ronca, E.; Kjønstad, E. F.; Rubio, A.; Koch, H. Coupled Cluster Theory for Molecular Polaritons: Changing Ground and Excited States. *Phys. Rev. X* **2020**, *10*, No. 041043.
- (127) Toida, H.; Nakajima, T.; Komiyama, S. Vacuum Rabi Splitting in a Semiconductor Circuit QED System. *Phys. Rev. Lett.* **2013**, *110*, No. 066802.
- (128) Guerin, W.; Santo, T.; Weiss, P.; Cipris, A.; Schachenmayer, J.; Kaiser, R.; Bachelard, R. Collective Multimode Vacuum Rabi Splitting. *Phys. Rev. Lett.* **2019**, *123*, No. 243401.
- (129) Hoffmann, N. M.; Schafer, C.; Rubio, A.; Kelly, A.; Appel, H. Capturing Vacuum Fluctuations and Photon Correlations in Cavity Quantum Electrodynamics with Multitrajectory Ehrenfest Dynamics. *Phys. Rev. A* **2019**, *99*, No. 063819.
- (130) Hoffmann, N. M.; Schäfer, C.; Säkkinen, N.; Rubio, A.; Appel, H.; Kelly, A. Benchmarking Semiclassical and Perturbative Methods for Real-Time Simulations of Cavity-Bound Emission and Interference. *J. Chem. Phys.* **2019**, *151*, 244113.
- (131) Schneider, R.; Domcke, W. S₁-S₂ Conical Intersection and Ultrafast S₂→S₁ Internal Conversion in Pyrazine. *Chem. Phys. Lett.* **1988**, *150*, 235–242.
- (132) Krempel, S.; Winterstetter, M.; Plöhn, H.; Domcke, W. Path-Integral Treatment of Multi-Mode Vibronic Coupling. *J. Chem. Phys.* **1994**, *100*, 926–937.
- (133) Worth, G. A.; Welch, G.; Paterson, M. J. Wavepacket Dynamics Study of Cr(CO)₅ after Formation by Photodissociation: Relaxation through an (E ⊕ A) ⊗ e Jahn-Teller Conical Intersection. *Mol. Phys.* **2006**, *104*, 1095–1105.
- (134) Worth, G. A.; Beck, M. H.; Jackle, A.; Meyer, H.-D. *The MCTDH Package*, Version 8.2 (2000). Meyer, H.-D. *The MCTDH Package*, Version 8.3 (2002), Version 8.4 (2007). Vendrell, O.; Meyer, H.-D. *The MCTDH Package*, Version 8.5 (2013). Version 8.5 contains the ML-MCTDH algorithm. See <http://mctdh.uni-hd.de>. Accessed on November 1st, 2023, used version: 8.5.14.
- (135) Colbert, D. T.; Miller, W. H. A Novel Discrete Variable Representation for Quantum Mechanical Reactive Scattering Via the S-Matrix Kohn Method. *J. Chem. Phys.* **1992**, *96*, 1982–1991.
- (136) Topaler, M.; Makri, N. Quantum Rates for a Double Well Coupled to a Dissipative Bath: Accurate Path Integral Results and Comparison with Approximate Theories. *J. Chem. Phys.* **1994**, *101*, 7500–7519.
- (137) A quote by Sidney Coleman states, “The career of a young theoretical physicist consists of treating the harmonic oscillator in ever-increasing levels of abstraction.” Similarly, we expect that isomorphic representations of the composite system in ever-increasing levels of abstraction are indispensable.